DOI:
10.1016/j.tox.2019.03.009

Document Version
Peer reviewed version

Ellipticine-loaded apoferritin nanocarrier retains DNA adduct-based cytochrome P450-facilitated toxicity in neuroblastoma cells

Radek Indra[a], Tereza Černá[a], Zbyněk Heger[b,c], Jan Hraběta[d], Marek Wilhelm[a], Simona Dostálová[b,c], Alžběta Lengálová[a], Markéta Martínková[a], Vojtěch Adam[b,c], Tomáš Eckschlager[d], Heinz H. Schmeiser[e], Volker M. Arlt[f,g], Marie Stiborová[a*]

[a]Department of Biochemistry, Faculty of Science, Charles University, Albertov 2030, 128 40 Prague 2, Czech Republic

[b]Department of Chemistry and Biochemistry, Mendel University in Brno, Zemedelska 1, 613 00 Brno, Czech Republic

[c]Central European Institute of Technology, Brno University of Technology, Purkynova 123, 612 00 Brno, Czech Republic

[d]Department of Pediatric Hematology and Oncology, 2nd Medical Faculty, Charles University and University Hospital Motol, 150 06 Prague; Czech Republic

[e]Division of Radiopharmaceutical Chemistry, German Cancer Research Center (DKFZ), Im Neuenheimer Feld 280, 69120 Heidelberg, Germany

[f]Department of Analytical, Environmental and Forensic Sciences, MRC-PHE Centre for Environment and Health, King's College London, 150 Stamford Street, London SE1 9NH, United Kingdom

[g]NIHR Health Protection Research Unit in Health Impact of Environmental Hazards at King's College London in partnership with Public Health England and Imperial College London, 150 Stamford Street, London SE1 9NH, United Kingdom

---

[*]**Corresponding author at**: Department of Biochemistry, Faculty of Science, Charles University, Albertov 2030, 128 40 Prague 2, Czech Republic

E-mail address: stiborov@natur.cuni.cz (M. Stiborová).

Abstract

Although ellipticine (Elli) is an efficient anticancer agent, it exerts several adverse effects. One approach to decrease the adverse effects of drugs is their encapsulation inside a suitable nanocarrier, allowing targeted delivery to tumour tissue whereas avoiding healthy cells. We constructed a nanocarrier from apoferritin (Apo) bearing ellipticine, ApoElli, and subsequently characterized. The nanocarrier exhibits a narrow size distribution suggesting its suitability for entrapping the hydrophobic ellipticine molecule. Ellipticine was released from ApoElli into the water environment under pH 6.5, but only less than 20% was released at pH 7.4. The interaction of ApoElli with microsomal membrane particles containing cytochrome P450 (CYP) biotransformation enzymes accelerated the release of ellipticine from this nanocarrier making it possible to be transferred into this membrane system even at pH 7.4 and facilitating CYP-mediated metabolism. Reactive metabolites were formed not only from free ellipticine, but also from ApoElli, and both generated covalent DNA adducts. ApoElli was toxic in UKF-NB-4 neuroblastoma cells, but showed significantly lower cytotoxicity in non-malignant fibroblast HDFn cells. Ellipticine either free or released from ApoElli was concentrated in the nuclei of neuroblastoma cells, concentrations of which being significantly higher in nuclei of UKF-NB-4 than in HDFn cells. In HDFn the higher amounts of ellipticine were sequestrated in lysosomes. The extent of ApoElli entering the nuclei in UKF-NB-4 cells was lower than that of free ellipticine and correlated with the formation of ellipticine-derived DNA adducts. Our study indicates that the ApoElli form of ellipticine seems to be a promising tool for neuroblastoma treatment.

Keywords: Ellipticine; Apoferritin nanoparticles; Cytochrome P450-mediated metabolism; DNA adducts; Neuroblastoma; Cytotoxicity.

Abbreviations: Apo, apoferritin; ApoElli, apoferritin-containing encapsulated ellipticine; CI, cell index; CYP, cytochrome P450; CTCF, corrected total cell fluorescence; DAP, 4',6-diamidino-2-phenylindole, dihydrochloride; DLPC, dilauroyl phosphatidylcholine; DLS, quasielastic dynamic light scattering; DMEM, Dulbecco's Modified Eagle Medium; DMSO, dimethyl sulfoxide; Elli, ellipticine; EPR, enhanced permeability and retention; GAPDH, glyceraldehyde 3-phosphate dehydrogenase; HDFn, neonatal human dermal fibroblasts; HPLC, high performance liquid chromatography; IMDM, Iscove's modified Dulbecco's medium; PEI, polyethylenimine; POR, NADPH:cytochrome P450 oxidoreductase; RAL, relative adduct labelling; RBC, red blood cells; RES, reticuloendothelial system; SCARA5, scavenger receptor class A member 5; TEM, transmission electron microscopy; TLC, thin-layer chromatography; TfR1. transferrin receptor 1.

1. Introduction

Ellipticine (5,11-dimethyl-6*H*-pyrido[4,3-*b*]carbazole, **Fig. 1**) and its derivatives are efficient anticancer agents that function through multiple mechanisms participating in cell cycle arrest and initiation of apoptosis (Auclair, 1987; Garbett et al., 2004; Kizek et al., 2012; Stiborova and Frei, 2014; Stiborová et al., 2011; 2015a). The main reason for the interest in ellipticine and its derivatives for clinical purposes is their high efficacy against several types of cancer (Auclair, 1987; Garbett et al., 2004; Kizek et al., 2012; Stiborova and Frei, 2014; Stiborová et al., 2011; 2015a). The predominant mechanisms of ellipticine's biological effects were proposed to be intercalation into DNA (Auclair, 1987; Garbett et al., 2004; Tmejova et al., 2014) and inhibition of topoisomerase II (Auclair, 1987; Garbett et al., 2004; Kizek et al., 2012; Stiborova and Frei, 2014; Stiborová et al., 2011; 2015a). We also showed that this antitumor agent forms covalent DNA adducts after metabolic activation by cytochrome P450 (CYP) enzymes and peroxidases (Stiborová et al., 2001, 2003a; 2003b; 2004; 2007a; 2007b; 2008; 2012b; Kotrbová et al., 2011), suggesting an additional DNA-damaging effect of ellipticine. This DNA damage has been found to be the major mechanism of ellipticine's antitumor activities (Stiborová et al., 2011; 2012b; 2014b; 2015a; Stiborova and Frei, 2014). Of the CYP enzymes, human CYP3A4 is the most active enzyme oxidizing ellipticine to 12-hydroxy- and 13-hydroxyellipticine, the reactive metabolites that dissociate to ellipticine-12-ylium and ellipticine-13-ylium which form two covalent DNA adducts (**Fig. 1**) (Stiborová et al., 2004; 2006; 2008; 2011; 2012a; 2012b; 2014b; 2015b). CYP3A4 also generates further metabolites such as 9-hydroxyellipticine, which is considered to be a detoxification metabolite as well as 7-hydroxyellipticine and ellipticine N^2-oxide (both minor metabolites) (Stiborová et al., 2004; 2011; 2012a; 2012b). 9-Hydroxyellipticine and 7-hydroxyellipticine are primarily generated by CYP1A1 whereas ellipticine N^2-oxide is mainly generated by CYP2D6 (**Fig. 1**) (Stiborová et al., 2004; 2011).

There are, however, several phenomena that can limit the clinical use of ellipticine and/or limit its anticancer efficiency. For instance, the clinical application of ellipticine is greatly limited by hydrophobicity and severe adverse toxic effects, including nephrotoxicity, hemolysis, xerostomia, hypertension, nausea and vomiting (Garbett and Graves, 2004; Stiborová et al., 2011; Stiborova and Frei, 2014). To some extent, the development of chemoresistance has been observed (Poljaková et al., 2009; Procházka et al., 2012; Hrabeta et al., 2015). One approach in mitigating these adverse effects is the encapsulation of ellipticine inside suitable nanocarrier, allowing targeted delivery to the tumor tissue while avoiding healthy cells (Chomoucka et al., 2010; Petros and DeSimone, 2010; Ali et al., 2011; Ryvolova

et al., 2012; Svenson, 2012; 2013; Dostalova et al., 2016). These nano-sized carriers can reach disease tissue and tumor cells *via* passive targeting (due to their size) (Dostalova et al., 2016) and/or active targeting (due to specific moieties on their surface) (Dostalova et al., 2016; Wu et al., 2012). Various materials have been tested for targeted ellipticine delivery, including peptide-based nanoparticles (Wu et al., 2012; Wan et al., 2016), polyHPMA-ellipticinium conjugates (Sedlacek et al., 2013), particles based on the triblock copolymer poly(ethylene oxide)-block-[tert-butylacrylamide-co-6-(N-methacryloylamino)-hexanoic acid hydrazide]-block-poly(ethylene oxide) (Studenovský et al., 2015) poly(ethylene oxide)-block-poly(allyl glycidyl ether) block copolymer-based micelles (P 1191 nanoparticles) (Stiborova et al., 2014a; 2015b), and octyl glucoside micelles (Gavvala et al., 2014). These nano-formulations seem to offer a promising way in overcoming some of the side effects of ellipticine (Sedlacek et al., 2013; Gavvala et al., 2014; Stiborova et al., 2014a; 2015b). Besides these nanocarriers, those prepared using ubiquitous proteins or protein cages also appear suitable for several anticancer drugs such as doxorubicin (Yang et al., 2007; Liang et al. 2014; Dostalova et al., 2016; 2017) and might therefore also be considered a suitable alternative for targeted ellipticine delivery. They are naturally biocompatible and biodegradable, and provide receptor-mediated passage through the cell membranes (Dostalova et al., 2016).

Apoferritin (Apo) is a naturally occurring iron-storage protein consisting of 24 protein subunits responsible for the storage and transfer of iron (Gallois et al., 1997; Kim et al., 2011; Kilic et al., 2012; Tmejova et al., 2013; Blazkova et al., 2013; Heger et al., 2014) that provides much needed properties of a drug-nanocarrier. Various ferritins are internalized by transferrin receptor 1 (TfR1) or scavenger receptor class A member 5 (SCARA5), overexpressed on membranes of some tumor cells (Mendes-Jorge et al., 2014). This can enable natural active targeting to those tumor cells, while passive targeting to tumor tissues is facilitated by the size of the ferritins (Blazkova et al., 2014; Heger et al., 2014). Apo protein subunits assemble to form a hollow cage with internal and external size of 8 and 12 nm in diameter, respectively, into which diverse low-molecular substances, such as drugs, can be placed (Uchida et al., 2007). It was shown that while disassembled, Apo protein subunits can be mixed with drug molecules and they are encapsulated within Apo cavity once reassembled (Blazkova et al., 2014; Heger et al., 2014). Using Apo as a nanocarrier has the potential to move undetected through the body without inducing any immune reaction. Furthermore, this natural protein can be modified with recognition ligands to achieve tumor-specific targeting (Dostalova et al., 2016; 2017). These extra modifications can avoid renal clearance and ensure enhanced permeability and retention

effect. However, they might disturb the Apo *in vivo* performance and biocompatibility due to altered surface physicochemical properties of ferritin (Dostalova et al., 2016).

The aim of this study was to construct a nanocarrier based on apoferritin-containing encapsulated ellipticine (ApoElli). Therefore, we developed a simple-to-use encapsulation protocol in this study to creating ApoElli. Further, the prepared ellipticine-bearing nanocarriers were characterized and their biochemical and cytotoxic properties investigated. We also studied the CYP-facilitated formation of ellipticine-derived DNA adducts using ApoElli.

2. Material and methods

2.1. Chemicals and reagents

Ellipticine, NADPH (as tetrasodium salt; ~98% purity), apoferritin (L-chain ferritin) from horse spleen, dilauroyl phosphatidylcholine (DLPC), glutathione, calf thymus DNA, and others were purchased from Sigma-Aldrich (St. Louis, MO, USA) in ACS purity (purity meets the standards of American Chemical Society), unless noted otherwise. Testosterone and 6-β-hydroxytestosterone were purchase from Merck (Darmstadt, Germany).

2.2. Enzymatic systems

Human CYP3A4 expressed in Supersomes™ (CYP3A4-Supersomes™), microsomes isolated from insect cells transfected with a baculovirus construct containing cDNA of human CYP3A4, NADPH:cytochrome P450 oxidoreductase (POR) and cytochrome b_5 (molar ratio of CYP3A4 to cytochrome b_5 of 1 to 5), were purchased from Corning (Tewksbury, MA, USA). The enzymatic activity of the experimental CYP3A4-Supersomes™ system used was verified by studying its efficiency to catalyze 6-β-testosterone hydroxylation, a marker reaction for CYP3A4 (see below).

2.3. Preparation of apoferritin-bound ellipticine

The stock solution of ellipticine (1 mg/ml) was prepared by dissolving ellipticine in distilled water with addition of 1 M HCl (at a ratio of water to HCl of 150 to 1). Ellipticine was encapsulated into apoferritin as follows: 200 µl of horse spleen Apo (50 mg/ml) was added to 2 ml of distilled water and 1 ml of ellipticine (1 mg). The pH was lowered from 6.7 to 2.7 by HCl to disassemble the Apo structure, and the mixture was shaken for 15 min to create a homogeneous solution. After mixing, the pH was adjusted again to neutral pH (7.2), by adding 7 µl of 1 M NaOH. The solution was mixed again for 15 min to enable the reassembly of the Apo molecule and encapsulation of ellipticine molecules within (creating ApoElli). The sample was diafiltrated three times with water using Amicon® Ultra - 0.5 ml 3K (Merck Millipore, Billerica, MA, USA) at 15,000*g* for 5 min. The parental molecule of ellipticine was stable under the conditions used for the preparation of ApoElli nanoparticles. The amount of ellipticine encapsulated in the Apo nanoparticles were determined using fluorescence detection (excitation wavelength 434 nm, emission wavelength 541 nm). The final concentration of ellipticine in ApoElli samples was 2.2 mM.

2.4. Characterization of ApoElli nanocarrier during storage

For every period of storage, aliquots were collected and prematurely released ellipticine was removed by diafiltration with distilled water using the Amicon® Ultra - 0.5 ml 3K (Merck Millipore, Billerica, MA, USA) at 13,000*g* for 15 min. The stability of ApoElli nanoparticles (1.7 mM stock solution) was determined after their incubation in distilled water at –20°C and/or +4°C for up to 10 weeks. Aliquots (150 µl) were diluted twice with water and diafiltrated using Amicon® Ultra - 0.5 ml 3K (Merck Millipore, Billerica, MA, USA) at 13,000*g* for 5 min. Ellipticine was extracted from 100 µl of ApoElli twice with 1 ml of ethyl acetate, the solvent was evaporated to dryness and residues were dissolved in 25 µl of methanol prior to analysis. Released and retained ellipticine was measured using HPLC as previously described (Stiborová et al., 2004; 2017).

Visualization and the average size of ApoElli nanocarriers prior to removal of released drug molecules and the Apo nanocarriers without ellipticine were performed using transmission electron microscopy (TEM) with negative staining technique. For this purpose, an organotungsten compound, Nano-W (Nanoprobes, Yaphank, NY, USA) was utilized. Then, 4 µl of samples was deposited onto 400-mesh copper grids coated with a continuous carbon layer. Dried grids were imaged by TEM (Tecnai F20; FEI, Hillsboro, OR, USA) at 80,000× magnification.

The average size of Apo and ApoElli was also determined by quasielastic dynamic light scattering (DLS) with a Zetasizer Nano ZS (Malvern Instruments, Worcestershire, UK). The nanocarrier was diluted to a concentration of 10 µg/ml of Apo, placed into polystyrene latex cells, and measured at a detector angle of 173°, wavelength of 633 nm, and temperature of 25°C, with refractive index of dispersive phase 1.45 and 1.333 for dispersive environment. For each measurement, Zen0040 disposable cuvettes (Brand GmbH, Wertheim, Germany) were used, containing 50 µl of sample. Equilibration time was 120 seconds. Measurements were performed in hexaplicate.

The surface zeta potential (ζ-potential) of the nanocarrier diluted to 20 µg/ml of Apo was measured using the Zetasizer Nano ZS (Malvern Instruments, Worcestershire, UK). For each measurement, disposable cells (DTS1070) were employed. The number of runs varied between 20 and 40, and calculations considered the diminution of particle concentration based on the Smoluchowski model, with an F(ka) of 1.5 and an equilibration time of 120 sec. Measurements were performed in triplicate.

2.5. The effect of pH on release of ellipticine from ApoElli nanoparticles

The released free ellipticine (from ApoElli) at different incubation times was determined by HPLC as previously described (Stiborová et al., 2004; 2017). To assay for the release of ellipticine, ApoElli sample (1.7 mM; 500 µl) were placed in a D-tube (molecular weight cut-off 3 kDa, D-Tube Dialyzer midi; (Novagen, Darmstadt, Germany) and incubated with gentle stirring in 14.5 ml of 0.1 M potassium phosphate buffer pH 6.5 and/or 7.4 at 37°C in the dark. 500 µl of buffer with released ellipticine was replaced and extracted twice with 1 ml of ethyl acetate at each time point. The solvent was evaporated to dryness and residues were dissolved in 25 µl of methanol before HPLC analysis.

2.6. Incubations to study 6-β-testosterone hydroxylation by CYP3A4 in Supersomes™

The incubation mixtures for measuring the testosterone metabolism contained in a final volume of 0.25 ml: 100 mM potassium phosphate buffer (pH 7.4 or 6.5), 50 µM testosterone (1.25 µl of stock methanol solution per incubation), 1 mM NADPH, and 100 nM human recombinant CYP3A4 in Supersomes™ with cytochrome b_5. The reaction was initiated by adding NADPH, the cofactor CYP-mediated enzyme system present in Supersomes™. Negative control reactions lacked either CYP3A4-Supersomes™ systems or cofactors or testosterone. After incubation for 15 min at 37°C, 5 µl of 1 mM phenacetin in methanol was added as an internal standard; testosterone oxidation was linear up to 30 min of incubation (data not shown). The reaction was terminated by the addition of 0.1 ml of 1 M aqueous Na_2CO_3 containing 2 M NaCl. The metabolites were extracted twice with 1 ml of dichloromethane and extracts were evaporated to dryness. The residues were dissolved in the mobile phase for HPLC (see below). Testosterone and its metabolite 6-β-hydroxytestosterone were separated on Nucleosil (C18) HPLC column (4.6 × 25 mm, 5 µm, Macherey-Nagel, Germany). The flow rates, mobile phases and detection wavelength were 0.6 ml per min, 65:35 methanol/H_2O (*v*/*v*), and 254 nm, respectively (Bořek-Dohalská et al., 2001; 2010).

2.7. Ellipticine release from ApoElli nanoparticles, its transfer into Supersomes™ containing human CYP3A4 and cytochrome b_5, and determination of its metabolism

Release of ellipticine from ApoElli nanoparticles in the presence of CYP3A4-Supersomes™ with cytochrome b_5, its transfer into these subcellular membrane particles and its ability to be metabolized were investigated in incubation mixtures of these particles in 0.1 M sodium phosphate buffer pH 6.5 and/or 7.4 for 20 min at 37°C. Incubation mixtures contained in a final volume of 0.25 ml: 100 mM potassium phosphate buffer (pH 6.5 or 7.4), 1 mM NADPH, 100 nM human recombinant CYP3A4 in Supersomes™ co-expressed with POR and cytochrome

b_5, and 25 μM free ellipticine or ApoElli. Stock solution of free ellipticine was 2.5 mM in dimethylsulfoxide (DMSO). Stock solution of Apo-bound form of ellipticine was 2.2 mM in water. The reaction was initiated by adding NADPH. Control incubations lacked either CYP3A4-Supersomes™, cofactor (NADPH), ellipticine or ApoElli. After incubation for 20 min at 37°C, 5 μl of 1 mM phenacetin in methanol was added as an internal standard. Ellipticine metabolites were extracted twice with 1 ml ethyl acetate, solvent was evaporated to dryness, residues were dissolved in 25 μl methanol and ellipticine metabolites were separated by HPLC as reported (Stiborová et al., 2004; 2017).

2.8. Ellipticine release from ApoElli nanoparticles and its transfer into liposomes

Liposomes are a form of vesicles mimicking the properties of microsomes that consist either of many, few or just one phospholipid bilayers. For the present study they were prepared as described previously (Stiborová et al., 2001) with minor modifications. Briefly, liposomes were prepared from dilauroyl phosphatidylcholine dissolved in chloroform (20 mg/ml). A lipid film was obtained by rotary evaporation of chloroform. Residual chloroform was removed by a stream of nitrogen. The lipid film was further dispersed with 0.1 M sodium phosphate buffer pH 7.4 and ultrasonicated twice at 20°C for 3 min each. In these vesicles amphiphilic and lipophilic molecules are solubilized within the phospholipid bilayer according to their affinity towards the phospholipids (Kulkarni et al., 2011). Because of these properties the possible transfer of ellipticine from ApoElli nanoparticles to these liposomes was tested. Appropriate amounts of ApoElli nanoparticles (2.2 mM ellipticine in ApoElli sample) were added to the prepared liposomes dispersed in 0.1 M sodium phosphate buffer pH 7.4 and the mixture was incubated for 20 min at 37°C. Liposomes were re-precipitated with 1 mM calcium chloride and centrifuged at 15,000*g* for 10 min as described (Kamath et al., 1971). Control incubations were carried out with the incubation mixture containing these components but in the absence of liposomes. The amounts of ellipticine present in the pellet of liposomes obtained by precipitation from the incubation mixture and in residual ApoElli nanoparticles retained in supernatant of these incubations were determined by HPLC (Stiborová et al., 2004; 2017). Likewise, the amounts of ellipticine present in pellet obtained by precipitation of the control incubation mixture (without liposomes) and in residual supernatant were determined by HPLC. Ellipticine from the samples was extracted twice with 1 ml ethyl acetate, solvent was evaporated to dryness, and residues were dissolved in 25 μl of methanol prior to HPLC analysis.

2.9. Determination of DNA adduct formation by ellipticine and ApoElli by ^{32}P-postlabeling

Incubation mixtures used to assess DNA adduct formation by ellipticine and ApoElli contained 0.5 mg protein of 100 nM human recombinant CYP3A4 in Supersomes™ with POR and cytochrome b_5 (500 nM), 0.1 mM ellipticine (dissolved in 7.5 µl DMSO) or ApoElli (in deionized water), and 0.5 mg of calf thymus DNA in a final volume of 0.75 ml as described previously for free ellipticine (Stiborová et al., 2004; 2012a; 2012b). The reaction was initiated by adding 0.1 mM ellipticine (in free or Apo-bound form) and incubations were carried out for 60 min at 37°C. Ellipticine-derived DNA adduct formation has been shown to be linear up to 90 min (Stiborová et al., 2004; 2012a; 2012b). Control incubations were carried out without CYP3A4-Supersomes™, or without NADPH, DNA, ellipticine or ApoElli. After incubation, DNA was isolated from the residual water phase by standard phenol/chloroform extraction. DNA adduct formation was analyzed using the nuclease P1 enrichment version of the ^{32}P-postlabeling assay (Stiborová et al., 2004; 2012a; 2012b). Resolution of the adducts by thin-layer chromatography (TLC) using polyethylenimine (PEI)-cellulose plates (Macherey and Nagel, Düren, Germany) was carried out as described (Stiborová et al., 2004; 2011; 2012a; 2012b). DNA adduct levels (RAL, relative adduct labeling) were calculated as described (Schmeiser et al., 2013).

2.10. Cell culture

The UKF-NB-4 cell line, established from bone marrow metastases of recurrent high-risk neuroblastoma, was a generous gift of Prof. Jindrich Cinatl, Jr. (University of Frankfurt, Germany). Neonatal human dermal fibroblasts (HDFn) were purchased from Thermo Fisher Scientific (Waltham, MA, USA). Cells were grown at 37°C and 5% CO_2, cultivated in Iscove's modified Dulbecco's medium (IMDM) with 10% fetal bovine serum and HDFn in DMEM (Dulbecco's Modified Eagle Medium) (all Life Technologies, Carlsbad, CA, USA). UKF-NB-4 and HDFn cells were cultivated for at least 48 hours with free ellipticine or ApoElli nanoparticles; this incubation time was chosen as it essentially corresponds to two rounds of cell division (Poljaková et al., 2009). Moreover, this time period is sufficient for ellipticine to enter the cells and trigger apoptosis (Kim et al., 2003; Poljaková et al., 2009).

2.11. AlamarBlue assay

Cytotoxicity of ellipticine and ApoElli nanoparticles in neuroblastoma UKF-NB-4 and non-malignant HDFn cells was determined in a 96-well plate format. For dose-response curves, cells were seeded in 100 µl of medium at a density of 1×10^4 UKF-NB-4 or 5×10^3 HDFn cells per well. Cells were treated with ellipticine or ApoElli nanoparticles (concentration of 0.04-20 µM)

and incubated for 48 hours. Cell viability was evaluated by the AlamarBlue assay as previously described (Plch et al., 2018). Briefly, after 48 hours incubation at 37°C in 5% CO_2, 5 µl of AlamarBlue (Thermo Fisher Scientific, Waltham, MA, USA) was added to each well and the plates were incubated for 2 hours. The fluorescence was measured using excitation wavelength of 570 nm and emission of 610 nm by SpectraMax® i3x Multi-Mode Microplate Reader (Molecular Devices, Sunnyvale, CA, USA). The (48 hours)-IC_{50} values were calculated from at least 3 independent experiments by SOFTmaxPro software.

2.12. Annexin V/DAPI double staining assay

For detection of apoptosis, Annexin V-Dy647 (Apronex s.r.o, Jesenice u Prahy, Czech Republic) staining was used according to the manufacturer's instructions and samples were analysed using flow cytometry (LSR II, BD, Franklin Lakes, CA, USA). Briefly, 8×10^5 UKF-NB-4 cells and 4×10^5 HDFn cells were plated in 60 mm dishes and treated with 5 µM ellipticine or ApoElli nanoparticles. After 48 hours incubation, cells were washed with PBS, trypsinized, collected by centrifugation and resuspended in 100 µl of Annexin binding buffer containing 1 µl of Annexin V-Dy647 and 10 µg/ml of 4',6-diamidino-2-phenylindole, dihydrochloride (DAPI, Thermo Fisher Scientific, Waltham, Massachusetts, USA), cells were gently vortexed and incubated for 15 min at room temperature in the dark. After incubation, cells were washed again in PBS and resuspended in 300 µl of binding buffer and measured using flow cytometer and subsequently analysed by FlowLogic software (Inivai Technologies, Mentone, Australia).

2.13. Cell cycle analysis

In order to evaluate cell cycle distribution, 8×10^5 UKF-NB-4 and 4×10^5 HDFn cells were plated in 60 mm dishes and exposed to 5 µM individual ellipticine forms and 5 µM ApoElli nanoparticles in deionized water. After 24 hours exposure, cells were collected by trypsinization, washed by PBS and fixed with 4% paraformaldehyde for 10 min. Thereafter these cells were permeabilised with 90% ice cold methanol and incubated at –20°C for a minimum of 1 hour. Samples were additionally incubated in DAPI (10 µg/ml) solution in dark under the laboratory temperature for 30 min, washed with PBS, and measured by flow cytometry employing LSR II flow cytometer and percentage of cells in G0/G1, S and G2/M was analysed with FlowLogic software (Inivai Technologies, Mentone, Australia).

2.14. Real-time monitoring of cell viability The xCELLigence RTCA DP Instrument (ACEA Bioscience Inc., San Diego, CA, USA) placed in a humidified incubator at 37°C and 5% CO_2 was used for real-time label free monitoring of cell viability (Ke et al., 2011). UKF-NB-4 cells (15,000 cells) were seeded into wells of 16-well plates for impedance-based detection. Cells were treated with 2.5 μM ellipticine or the same concentrations of ellipticine in ApoElli nanoparticles. The cell index (CI) was monitored every 30 min for 148 hours and data was recorded by the supplied RTCA software.

2.15. Histone H2AX phosphorylation status

To determine phosphorylation of histone H2AX, 8×10^5 UKF-NB-4 and 4×10^5 HDFn cells were plated in 60 mm dishes and treated with 5 μM ellipticine or ApoElli nanoparticles for 48 hours. After treatment, cells were washed and subsequently fixed in 4% formaldehyde in PBS for 10 min. After washing with PBS, cells were re-suspended in ice cold 90% methanol and incubated for 1 hour at –20°C. Cells were washed three times with wash buffer (PBS containing 0.5% BSA and 0.2% Triton X) and then incubated in 50 μl of wash buffer containing 5 μl of γH2AX antibody (Alexa Fluor® 647 anti-H2AX-Phosphorylated (Ser139), Biolegend, San Diego, CA, USA) for 60 min at 4°C. Cells were washed, measured using a LSR II flow cytometer (BD, Franklin Lakes, CA, USA) and analysed with FlowLogic software.

2.16. Confocal microscopy

5×10^5 UKF-NB-4 or 2.5×10^5 HDFn cells were grown on 35 mm glass bottom culture dishes (In Vitro Scientific, Sunnyvale, CA, USA) for 24 hours before treatment with 10 μM ellipticine or 10 μM ApoElli for 2 hours at 37°C and observed with a laser-scanning confocal microscope, Leica TCS SP8 (Leica Microsystems GmbH, Wetzlar, Germany). For excitation of the ellipticine, laser with wavelength of 488 nM was used; emitted light was collected in the range of 552–638 nM. All images were recorded with a ×100 objective and using the Leica Application Suite X (LAS X) system. Nuclear fluorescence intensity of ellipticine was evaluated with the image analysis software ImageJ (NIH, Bethesda, USA) and calculated as the corrected total cell fluorescence (CTCF), using the formula CTCF = Integrated Density – (Area of selected nuclei × Mean fluorescence of background readings).

2.17. Analysis of cellular ellipticine

The day before analysis, UKF-NB-4 cells were seeded at 1×10^4 UKF-NB-4 and HDFn at 5×10^3 cells per well in 96-well plate. Cells were treated with 10 μM ellipticine or 10 μM ApoElli for

2 hours at 37°C and fluorescence intensity of ellipticine was measured (excitation wavelength 434 nm, emission wavelength 541 nm) with a SpectraMax® i3x Multi-Mode Microplate Reader (Molecular Devices, Sunnyvale, CA, USA) in individual cells using imaging cytometer module.

2.18. Red blood haemolytic test

The haemolytic assay was conducted to evaluate the haemocompatibility of Apo and ApoElli on erythrocytes from human donor with signed informed consent. Plasma from a fresh blood sample was removed by multiple washing with 150 mM sodium chloride and centrifugation at 3000 rpm for 10 min. Then different concentrations of Apo and ApoElli (6.3-100 µM ellipticine in ApoElli and 13.8-220 µg/l Apo) in PBS pH 7.4 were mixed with the red blood cells (RBC) and incubated for 1 hour at 37°C. PBS and 0.1% Triton X-100 was used as negative and positive control, respectively. After completion of the incubation period, the cells were centrifuged and the absorbance of the supernatant containing lysed erythrocytes was measured at 540 nm. The percentage of haemolysis was determined by the following equation:

$$\% \text{ Haemolysis} = \frac{(A_t - A_c)}{(A_{100\%} - A_c)} \times 100$$

where A_t is the absorbance of the supernatant from samples incubated with the particles; A_c is the absorbance of the supernatant from negative control (PBS) and $A_{100\%}$ is the absorbance of the positive control supernatant (completely lysed RBC incubated in the presence of 0.1% Triton X-100) (Goswami et al., 2015).

2.19. Western blot analysis of SCARA5

1×10^6 cells of each cell line (UKF-NB-4 and HDFn cells) was harvested by trypsinization, then centrifuged at 200 rcf for 10 min and washed with PBS with subsequent centrifugation at 200 rcf for further 10 min. The pellet was resuspended in 100 µl of ice-cold RIPA lysis buffer (20 mM Tris-HCl, pH 7.5, 150 mM NaCl, 1 mM Na_2EDTA, 1 mM EGTA, 1% NP-40, 1% sodium deoxycholate, 2.5 mM sodium pyrophosphate, 1 mM glycerophosphate, 1 mM Na_3VO_4, 1 µg/ml leupeptin) containing 1 µl of protease inhibitor cocktail (Sigma-Aldrich, St. Louis, MO, USA) and vortexed for 15-30 sec. Lysis was then performed on ice for 45 min. Lysate was sonicated 5 times for 3 sec to remove genomic DNA. After centrifugation for 10 min at 22 000 rcf, the supernatant containing proteins was stored at −80°C until analysis. 10 µl containing 10 µg of proteins was mixed with 5 µl of non-reducing SDS-PAGE loading buffer prior to

separation on 12.5% SDS-PAGE at 200 V for 35 min. Proteins were electroblotted onto a PVDF membrane. The PVDF membrane was blocked with 5% bovine serum albumin in PBS (37 mM NaCl, 2.7 mM KCl, 1.4 mM NaH_2PO_4, 4.3 mM Na_2HPO_4, pH 7.4) and then incubated separately with primary antibodies against SCARA5 (1 µg/ml = 1:1000, ab118894, Abcam), or glyceraldehyde 3-phosphate dehydrogenase (GAPDH) G-9 (1:700, sc-365062, Santa Cruz Biotechnology) at 4°C overnight. Next, the membranes were incubated with horseradish peroxidase (HRP)-labelled secondary antibodies (goat anti-mouse P0260 [Dako] for GAPDH, 1:5000 or goat anti-rabbit SAB3700831 [Sigma Aldrich] for SCARA5, 1:5000) for 1 hour at 25°C. Chemiluminiscent detection was performed using Clarity Western ECL Blotting Substrate (Bio-Rad, CA, USA) and bands were analysed using Azure c600 imager (Azure Biosystems, Dublin, CA, USA). The membranes were visualized and processed using Azure c600 (Azure Biosystems, Dublin, CA, USA).

2.20. Detection of ellipticine-DNA adducts in UKF-NB-4 cells by ^{32}P-postlabeling

Neuroblastoma UKF-NB-4 cells were seeded 24 hours prior to treatment at a density of 1×10^5 cells/ml in three 75 ml culture flasks in a total volume of 20 ml of IMDM. Cells were treated with 5 µM ellipticine or 5 µM ApoElli nanoparticles for 48 hours. Cells were harvested after trypsinizing by centrifugation at 2,000×*g* and washed twice with 5 ml of PBS yielding a cell pellet which was stored at –80ºC until DNA isolation. DNA was isolated using a standard phenol-chloroform extraction method as described (Frei et al., 2002; Poljaková et al., 2007; 2009; Stiborova et al., 2015a). Ellipticine-DNA adducts were detected and quantified using the nuclease P1 enrichment version of the ^{32}P-postlabeling assay as described previously for *in vitro* (Frei et al., 2002; Poljaková et al., 2007; 2009; Stiborova et al., 2015a) and *in vivo* analyses (Stiborová et al., 2003a; 2003b; 2008; 2011; 2014a).

2.21. Statistical analysis

Data are expressed as mean ± SD. Data was analysed using GraphPad Prism 7 using ANOVA with post-hoc Tukey HSD Test. *P* value < 0.05 was considered as significant.

3. Results and discussion

3.1. Preparation of apoferritin-bound ellipticine (ApoElli) nanoparticles

Apoferritin (Apo) is known to reversibly dissociate and associate, which are processes dependent on pH (Kim et al., 2011). When Apo is disassembled after mixing it with drug molecules, these molecules can encapsulate within the Apo cavity once reassembled (Kilic et al., 2012; Blazkova et al., 2013; Tmejova et al., 2013). As shown in **Fig. 2** we utilized this easy-to-use encapsulation protocol to prepare Apo nanoparticles encapsulated with the anticancer agent ellipticine (ApoElli). The ellipticine concentration in the prepared ApoElli nanoparticles was 2.2 mM.

Size is one of the most important parameters influencing the *in vivo* biodistribution of nanocarriers and has a great impact on the mode of cellular internalization (Petros and DeSimone, 2010). Nanocarriers with the size of 20-100 nm are considered best suitable for enhanced permeability and retention (EPR) effect (Svenson, 2016), while avoiding extravasation from normal blood vessels which occurs only with particles below 10 nm (Appelbe et al., 2016). This also avoids removal from the body through renal clearance for particles below 5 nm or elimination by the reticuloendothelial system (RES) which traps particles above 100 nm (Liu et al., 2016). Visualization of the ApoElli nanocarriers and determination of their size prior to removal of released drug molecules and the Apo nanocarriers without ellipticine were performed using TEM (**Fig. 3A**) and DLS (**Fig. 3B**). The average size of Apo and ApoElli nanoparticles determined by DLS were 11.7 ± 0.31 (n=6) and 10.1 ± 0.57 nm (n=6), respectively (**Fig. 3B,C**). Even though the reasons for these small differences between Apo and ApoElli nanoparticles still needs to be explained, one can speculate that they can result from the process of encapsulation. Specifically, some Apo subunits seem not to be properly reassembled and thus remain in solution. Their size might thereafter decrease the analysed value of the average size of ApoElli. However, this suggestion remains to be confirmed in future investigations. The lower size of ApoElli particles than those of Apo is not seen using TEM without a high resolution module (**Fig. 3**).

We also utilized the DLS method to determine the polydispersive index and the surface ζ-potential of the prepared nanoparticles. The polydispersive index is used as a measure of the breadth of molecular weight distribution of polymers. For Apo and ApoElli nanoparticles this was 0.350 ± 0.09 (n=6) and 0.419 ± 0.24 (n=6), respectively (**Fig. 3C**), indicating very well homodispersed systems (Gaumet et al., 2008). The surface ζ-potential of Apo and ApoElli nanocarriers showing the electrostatic potential at the electrical double layer surrounding both nanoparticles in solution was also characterized. The average values of -32.0 ± 2.02 (n=6) and -36.2 ± 2.65 (n=6) for Apo and ApoElli, respectively (**Fig. 3C**), indicate that they are strongly

anionic (Clogston and Patri, 2011). High values of ζ-potential result in strong repulse moments among the particles leading to the stability of these colloidal disperse systems.

Next we evaluated the stability of ApoElli (i.e. the degree of ellipticine release) at two different temperatures (–20°C and +4°C) for up to 10 weeks. As shown in **Figure 4A**, ApoElli was stable for up to 10 weeks of storage at +4°C. Essentially no ellipticine was released under these storage conditions whereas ellipticine was markedly released during storage at –20°C; 25% and 60% of ellipticine is released from ApoElli in 2 and 10 weeks, respectively.

One of the reasons that Apo was chosen in our experiments was its ubiquitous presence in nature and its natural property to self-assemble into uniform icosahedral nanocages that are highly stable and do not form aggregates in the physiological environment (Gallois et al., 1997). Using TEM, we essentially found no changes in aggregation of ApoElli nanocarriers as well in their shape and size after storage for 28 days at +4°C (compare **Figs. 3Ab** and **3Ac**).

All these findings demonstrate that the prepared ApoElli nanoparticles with the average size of 10.1 ± 0.57 (n=6) nm form a homogenous system with a low polydispersity and high colloidal stability. This suggests their high suitability for nanomedicine; for example because of their stability during the storage and the size appropriate for EPR internalization (Moore et al., 2015)

3.2. Release of ellipticine from ApoElli nanoparticles

To investigate the release of ellipticine from ApoElli nanoparticles they were incubated either at pH 6.5 or pH 7.4 for 48 hours at 37°C and the release of ellipticine was subsequently monitored using HPLC. The release of ellipticine from the ApoElli nanoparticles proceeded in two stages: an initial rapid release was followed by a phase of slow and long-lasting release of ellipticine (**Fig. 4B**). At pH 7.4 ApoElli nanoparticles were essentially stable; less than 20% release of free drug was found over 48 hours of incubation. In contrast, at pH 6.5 ellipticine release was detected with a half-life of 7 hours and the maximum release of 83 ± 7% was reached after 48 hours (**Fig. 4B**). The pH-dependent release of ellipticine might be caused by at least two reasons. First, at pH 6.5 changes in the ApoElli structure might occur resulting in disintegration of Apo to its subunits (see scheme in **Fig. 2**) (Kim et al., 2011). This is a typical feature for pH-related changes to_the peptide/apoferritin nanoparticle structure (Kim et al., 2011; Zhang et al., 2019). Second, the ellipticine as a hydrophobic base compound is easily released from the ApoElli nanoparticles into the water environment under the acidic conditions. These acidic conditions are typical for tumor microenvironments (Corbet and Feron, 2017).

3.3. Ellipticine release from ApoElli in the presence of CYP3A-Supersomes™, its transfer into these subcellular particles and its oxidation by this enzymatic system

Incubations of both free ellipticine and ApoElli with Supersomes™ containing human CYP3A4, POR and cytochrome b_5 were employed to analyze the transfer of ellipticine from both forms of this drug into these subcellular membrane particles. For this purpose we studied the CYP3A4-facilitated metabolism of free and ApoElli bound ellipticine. In order to evaluate the suitability of CYP3A4-Supersomes™ for our experiments, we tested the system to catalyze testosterone 6-β-hydroxylation as a marker for CYP3A4 enzyme activity (Bořek-Dohalská et al., 2001). As shown in **Figure 5A** our results demonstrated that the Supersomal CYP3A4 system can catalyze this marker reaction and thus we can argue that CYP3A4-Supersomes™ are a suitable system for our enzymatic studies.

CYP3A4-Supersomes™ incubated with free ellipticine in the presence of NADPH were capable of oxidizing ellipticine to 9-hydroxy-, 12-hydroxy- and 13-hydroxyellipticine (**Fig. 5B)**; NADPH acts as cofactor for the CYP-mediated enzyme system present in Supersomes™. The same metabolites were also generated in the presence of ApoElli nanoparticles in the incubation mixtures instead of free ellipticine. Beside these ellipticine oxidation products, two other metabolites, 7-hydroxyellipticine and ellipticine N^2-oxide were also detectable. However, their amounts were quite low (if detectable) and therefore were not quantified. The oxidation of free ellipticine and ApoElli was pH-dependent. By lowering pH from 7.4 to 6.5 oxidation of ellipticine was decreased; the amounts of ellipticine metabolites were up to 5-times lower at pH 6.5 than pH 7.4 (**Fig. 5B**). The effect of the pH on CYP3A4-mediated catalysis was confirmed by measuring testosterone 6-ß-hydroxylation. Our results indicated that this reaction was also decreased at low pH, but this effect was less pronounced compared to ellipticine oxidation (compare **Figs. 5A** and **5B**).

Interestingly, at pH 7.4 the amounts of ellipticine metabolites generated by CYP3A4 in the presence of NADPH were similar regardless of either form of ellipticine (free ellipticine and ApoElli) (**Fig. 5B**). Although ApoElli nanoparticles are stable at this pH (see **Fig. 4B**), the generation of ellipticine metabolites indicated that this drug is efficiently released from the apoferritin cage in ApoElli nanoparticles not only at pH 6.5, but even at pH 7.4. The amounts of ellipticine metabolites formed from ApoElli were only up to 1.4-fold lower compared to those formed from free ellipticine at both pH levels. This finding indicates that the presence of the microsomal membrane of Supersomes™ is much more important for ellipticine release from ApoElli in this enzyme system than pH. The properties dictated by the phospholipid bilayer

forming the microsomal membrane of CYP3A4-Supersomes™ might be responsible for this unique phenomenon that has not been described yet. Interaction of ApoElli nanoparticles with Supersomes™ might result in the release of ellipticine from these nanoparticles entering the supersomal membrane system. In order to investigate this possibility we prepared liposomes mimicking the properties of microsomal membrane particles and incubated them with ApoElli nanoparticles in order to evaluate the amounts of ellipticine released from ApoElli transported to these liposomes. As shown in **Figure 6** ellipticine was released from ApoElli nanoparticles and entered the liposomes, supporting the above mentioned hypothesis.

All these results indicated that both free ellipticine and ellipticine released from ApoElli nanoparticles are capable of entering the system containing the membrane of endoplasmic reticulum, where it can be metabolized by the CYP3A4-mediated enzymatic system.

3.4. Formation of ellipticine-derived-DNA adducts from free ellipticine and ApoElli nanoparticles by CYP3A-Supersomes™

In further experiments using CYP3A4-Supersomes™ in the presence of DNA we analyzed the formation of ellipticine-derived DNA adducts of free ellipticine and ApoElli. These experiments were carried out to prove the release of ellipticine from ApoElli, its transfer to CYP3A4-Supersomes™ and its oxidation by this enzymatic system using a further independent approach. As shown in **Figure 1** the oxidative activation of ellipticine to the DNA reactive metabolites 13-hydroxy- and 12-hydroxyellipticine is catalyzed by several human CYP enzymes including CYP3A4 (Stiborová et al., 2012b). Ellipticine-derived DNA adduct formation was detected and quantified using the ^{32}P-postlabeling method (**Fig. 5C**). One major DNA adduct was detected (see insert of **Figure 5C**) and was generated at both pH 6.5 and 7.4. This adduct spot was shown previously to be formed from ellipticine-13-ylium generated by decomposition of 13-hydroxyellipticine (**Fig. 1**) (Stiborová et al., 2004). These results confirmed again that ellipticine can be released from ApoElli particles at pH 7.4, when Supersomal microsomes were present in the test system. Adduct 2 generated from 12-hydroxyellipticine (**Fig. 1**) was not detectable under the experimental conditions (i.e. CYP3A4-Supersomes™) used (**Fig. 5C**). No adducts were detected in control incubations, where Apo nanoparticles without encapsulated ellipticine were present or in the absence of free ellipticine (**Fig. 5C**).

In CYP3A4-Supersomes™ apoferritin-bound ellipticine generated up to 2.5-fold lower levels of DNA adducts than free ellipticine (**Fig. 5C**). The lower DNA adducts levels formed from ApoElli nanoparticles could not be explained by the amounts of ellipticine metabolites

formed from ApoElli as these were only up to 1.4-fold lower as compared to those formed from free ellipticine (compare **Figs. 5B** and **5C**). This is probably caused by the presence of Apo protein retaining in the incubation mixture after ellipticine release from the ApoElli nanoparticles and thus this protein can compete with DNA to react with reactive ellipticine intermediates (i.e. ellipticine-13-ylium) forming ellipticine-derived protein (Apo) adducts instead of DNA adducts. Indeed, the formation of ellipticine-derived protein adducts has been shown previously demonstrating that activated ellipticine can efficiently bind to several proteins (Martínek et al., 2010).

3.5. Analysis of internalization of free ellipticine and ApoElli nanoparticles into UKF-NB-4 and HDFn cells

One of the most important properties of nanocarriers is their ability to internalize into target cells and the ability of its cargo to reach the cell organelle(s) where it can effectively inhibit the cell growth (Stylianopoulos and Jain, 2015). Therefore, we tested the internalization of ApoElli into the cancer cells and as a model we used the neuroblastoma UKF-NB-4 cell line, which was previously found to be sensitive to ellipticine treatment (Poljakova et al., 2009; 2011; Hrabeta et al., 2015). Neuroblastoma UKF-NB-4 cells were also chosen as a model because they not only overexpress TfR1 (Krausova, 2017), a cell membrane-associated glycoprotein responsible for incorporation of H-chain ferritin through an endocytic process (Uchida et al., 2007; Nakamura et al., 2012), but also SCARA5 for L-chain ferrritin (Uchida et al., 2007). Indeed, as shown in **Figure 7A**, SCARA5 was highly expressed in UKF-NB-4 cells, in contrast to normal human fibroblast HDFn cells which were used as a model for non-malignant cells. Both cell lines were treated with ellipticine, either free or encapsulated in ApoElli, and their effects on these cells were investigated.

Subcellular localization of ellipticine after treatment was analyzed by confocal microscopy demonstrating that both forms of ellipticine enter UKF-NB-4 and HDFn cells (**Fig. 7B**). As an indicator of ellipticine concentrations we measured the fluorescence intensity of ellipticine in whole cells (total) which was higher in HDFn cells than in UKF-NB-4 cells; in both cell lines the cellular ellipticine concentration was lower after ApoElli compared to free ellipticine treatment (**Fig. 7C**). No ellipticine fluorescence was detectable in the membranes of the tested cells (**Fig. 7B**). This indicates that both forms of ellipticine (free ellipticine and ApoElli) overcome the plasmatic membranes of these cells. The higher uptake of free ellipticine than ApoElli can be explained by the high hydrophobicity and the small size of this drug, which both dictates the easy transfer of free ellipticine across cell membranes, as compared to the

transport of the more polar and high-molecular ApoElli compound. As described previously (Zhang et al., 2016), the passive diffusion pathway is responsible for the transport of free ellipticine into the cells. In contrast, the size and anionic properties of ApoElli nanoparticles (**Fig. 3**) prevent such a type of transport. Therefore, endocytosis, a typical process of transport of particles into cells (Uchida et al., 2007; Nakamura et al., 2012), seems to play a predominant role in the transport of ApoElli across the cell membrane in the tested cells. Nevertheless, further investigations are needed to confirm this suggestion but were beyond the scope of the present work.

Neuroblastoma UKF-NB-4 cells treated with either free ellipticine or ApoElli nanoparticles showed that ellipticine fluorescence was mainly located in cell nuclei in contrast to non-malignant HDFn cells; ellipticine fluorescence was more than 2-fold higher in the nuclei of UKF-NB-4 cells than in HDFn cells (**Figs. 7B** and **7D**). In non-malignant HDFn cells most of ellipticine was located in the lysosomes after the uptake of free ellipticine and ApoElli (**Figs. 7B** and **7D**). These results demonstrate that both forms of ellipticine are taken up by the cell models but accumulate it in different compartments depending on the cell type. The lower fluorescence intensity of ellipticine in the cells exposed to ApoElli compared to cells exposed to free ellipticine might be caused not only by an easier entry of ellipticine into the cells than ApoElli as mentioned above, but might also be caused by a slower release of ellipticine from ApoElli. The amounts of ellipticine are partially retained in ApoElli nanoparticles. This suggestion is supported by the results from experiments investigating the release of ellipticine form ApoElli in the presence of liposomes or CYP3A4-Supersomes^{TM} (see **Figs. 5** and **6**).

3.6. Cytotoxicity and induction of apoptosis by ellipticine and ApoElli nanoparticles in UKF-NB-4 and HDFn cells, and their effects on cell cycle distribution

We measured the cytotoxicity of free ellipticine and ApoElli in UKF-NB-4 and HDFn cells using the AlamarBlue viability assay and/or real-time label-free monitoring of cell impedance. Apo nanoparticles where ellipticine was not present were not toxic in both cell lines (data not shown).

Using the AlamarBlue viability assay the IC_{50} values of ellipticine in UKF-NB-4 and HDFn cells treated with free ellipticine were 1.1±0.05 and 2.6±0.2 μM, respectively, whereas for ApoElli nanoparticles the IC_{50} values were 1.4±0.1 and 2.9±0.3 μM, respectively (**Figs. 8A** and **8B**). These findings indicate that non-malignant HDFn cells are less sensitive to ellipticine treatment than neuroblastoma UKF-NB-4 cells. This might be explained by ellipticine compartmentalization in both cell types; higher levels of ellipticine were located in nuclei of

UKF-NB-4 cells, the target compartment for its cell toxicity (Stiborova and Frei, 2014), while in HDFn cells it is efficiently internalized into lysosomes, thereby decreasing its cell toxicity (Hrabeta et al., 2015).

As shown in **Figure 8C**, apoptosis was induced in UKF-NB-4 cells after treatment with 5 μM ellipticine and ApoElli form. However, the potency to induce apoptosis was lower after exposure to ApoElli nanoparticles than free ellipticine. These results are consistent with lower amounts of ellipticine (determined by its fluorescence) in the nuclei of these neuroblastoma cells after treatment with ApoElli than with free ellipticine (see **Fig. 7D**). In contrast, no apoptosis was observed in treated HDFn cells (**Fig. 8D**).

To evaluate the toxicity of the ApoElli nanocarrier to other non-malignant cells we performed a haemocompatibility assay in human RBC. For this purpose we used fresh blood from a human donor with absorbance measurement and visualization in ambient light of lysed RBC (**Fig. 8G**). The ApoElli formulation showed excellent haemocompatibility. Likewise, control Apo (i.e. without encapsulated ellipticine) exhibited excellent haemocompatibility (data not shown).

In further experiments we studied the cell cycle distribution of UKF-NB-4 and HDFn cells after exposure to ellipticine and ApoElli nanoparticles. Compared to controls (i.e. untreated cells) exposure to both forms of ellipticine resulted in increased S and/or G2/M phase arrest in UKF-NB-4 cells; this effect was not seen in HDFn cells (**Figs. 8E** and **8F**). In contrast, HDFn cells arrested in G0/G1 phase after ellipticine and ApoElli treatment (**Fig. 8F**) which resulted in essentially no cell growth. This feature was the reason that the cytotoxic potency of ellipticine and ApoElli in HDFn cells could not be analyzed using the xCELLigence system. But this method was used to test the cytotoxicity of ellipticine and ApoElli in UKF-NB-4 cells (**Fig. 9**). UKF-NB-4 cells cultured in the presence of 2.5 μM ellipticine and the same concentration of this drug present in ApoElli grow exponentially up to 116 hours in culture. Treatment of UKF-NB-4 cells with 2.5 μM ApoElli nanoparticles for 48 hours resulted in a 1.3-fold decrease in the value of cell index as compared to treatment with free ellipticine (**Fig. 9**).

3.7. The effect of treatment of UKF-NB-4 and HDFn cells with ellipticine and ApoElli nanoparticles on phosphorylation of H2AX histone protein

One of the DNA-damaging mechanisms leading to ellipticine cytotoxicity is based on the inhibition of topoisomerase II generating double-strand DNA breaks (Zwelling et al., 1982). Therefore, we examined the ability of ellipticine and ApoElli nanoparticles to induce double-strand DNA breaks in UKF-NB-4 and HDFn cells. Phosphorylation of histone H2A on serine

139, termed γH2AX, by kinases sensing double-strand DNA breaks is a sensitive marker of this type of DNA damage (Nakamura et al., 2010; Sharma et al., 2012). UKF-NB-4 and HDFn cells were treated with 5 μM ellipticine or ApoElli and the levels of γH2AX were examined by flow cytometry. Whereas essentially no phosphorylation of H2AX was observed after treatment in HDFn with either ellipticine or ApoElli, increased γH2AX levels were detectable in UKF-NB-4 cells (**Fig. 10A**). This finding confirmed that free ellipticine or ApoElli is transported into cancer cells where it can reach DNA in the nucleus to cause double-strand DNA breaks. The lower compartmentalization of ellipticine in the nuclei of non-malignant HDFn cells explains the lack of this DNA damage in these cells.

The percentage of cells with γH2AX did not correlate with the cytotoxicity of ellipticine and ApoElli as measured by AlamarBlue assay or Annexin V positive/DAPI positive cells (compare **Figs. 8** and **10**). The levels of DNA double-strand breaks in UKF-NB-4 cells were ~1.3-times higher after their treatment with ApoElli compared to free ellipticine. Hence, ellipticine-induced cytotoxicity and apoptosis in neuroblastoma UKF-NB-4 cells after exposure to ApoElli seems to be linked not only to the induction of DNA double-strand-breaks, but also to other types of DNA damage. In order to shed more light on this phenomenon, additional experiments were conducted to investigate covalent ellipticine-derived DNA adduct formation in UKF-NB-4 cells, in which ellipticine accumulates in the nuclei.

3.8. The effect of treatment of UKF-NB-4 cells with ellipticine and ApoElli nanoparticles on the formation of covalent ellipticine-derived DNA adducts

Ellipticine-mediated cytotoxicity is predominantly linked to covalent DNA adducts formed during enzymatic CYP- and peroxidase-catalyzed activation of ellipticine (Stiborová et al., 2011; Stiborová and Frei, 2014). Therefore, we investigated the generation of ellipticine-DNA adducts in UKF-NB-4 cells (sensitive to ellipticine) exposed to ellipticine and ApoElli nanoparticles. As done in experiment with CYP3A4-Supersomes^{TM} (see **Figure 5C**) we again employed the ^{32}P-postlabeling assay. As shown in **Figure 10B** two major DNA adducts were observed in UKF-NB-4 cells after exposure to free ellipticine or ApoElli nanoparticles. Adducts 1 and 2 are generated from the ellipticine metabolites 13-hydroxyellipticine and 12-hydroxyellipticine, respectively (Stiborová et al., 2004; 2007a).

The levels of covalent ellipticine-derived DNA adducts in UKF-NB-4 cells correlated with the amounts of ellipticine in the nuclei of these cells; the levels of ellipticine-DNA adducts generated by ApoElli were up to ~70% of those formed by free ellipticine (see **Figure 10B**). Adduct levels not only correlated with the cytotoxicity of ellipticine and ApoElli in UKF-NB-

4 cells as measured by AlamarBlue viability assay (**Figs. 8A** and **8B**) but also with the degree of apoptosis induced by ellipticine and ApoElli in these cells (**Figs. 8C** and **8D**). These results demonstrate that the formation of covalent ellipticine-derived DNA adducts seems to be predominantly responsible for the toxic effects of ellipticine in UKF-NB-4 cells and this conclusion is in accordance with other studies (Stiborová and Frei, 2014, Stiborová et al., 2014b).

Again, these results also demonstrate that ellipticine and ApoElli might, when transported into the target cells, enter these cells to cause DNA damage in the nucleus. The mechanism of the uptake of free ellipticine and the ApoElli nanoparticles across the membrane is probable by diffusion and endocytosis, respectively. However additional experiments will be necessary in the future to better understand this process.

4. Conclusions

Apoferritin can be used to effectively delivery the anticancer agent ellipticine into cancer cells. We showed that ellipticine can be encapsulated by apoferritin and subsequently be released from its ApoElli form. Furthermore, a unique finding of our study is that ApoElli is capable of transferring ellipticine into microsomal subcellular particles, where it is oxidized by the CYP-mediated system to generate reactive hydroxylated metabolites able to form covalent DNA adducts. These adducts are also generated in neuroblastoma UKF-NB-4 cells exposed to both free ellipticine and ApoElli nanoparticles. We showed that the cytotoxicity of ApoElli is lower than that of the free form of ellipticine. However, more importantly, whereas ApoElli nanoparticles were toxic in neuroblastoma UKF-NB-4 cells, their toxicity in non-malignant fibroblastic HDFn cells were significantly lower. This implies the suitability of ApoElli to inhibit the growth and development of tested cancer cells. Compartmentalization of ellipticine in the nuclei of neuroblastoma UKF-NB-4 cells after treatment with both forms of ellipticine was responsible for the induced DNA damage (i.e. DNA-double-strand-breaks and formation of covalent ellipticine-derived DNA adducts) in these cancer cells. Covalent modification of DNA seems to be the critical factor dictating the observed cytotoxicity. In contrast to drug internalization into the nuclei of UKF-NB-4 cells, high amounts of ellipticine are sequestrated in lysosomes in fibroblastic HDFn cells. The latter effect is responsible for the lower concentration of ellipticine in the nuclei resulting in lower cytotoxicity and/or no apoptosis in these non-malignant cells.

In conclusion, we propose that apoferritin with encapsulated ellipticine might be a suitable carrier to target several cancer cells including neuroblastoma. The receptors TfR1/SCARA5

which are commonly over-expressed in these cancer cells might help to achieve this targeting without the need to introduce additional moieties on the surface. Therefore, this nanoparticle form of ellipticine seems to be a promising tool for cancer treatment.

Acknowledgements

Work at Charles University was supported by the Grant Agency of the Czech Republic (grant GACR 17–12816S) and the Charles University in Prague (grant GAUK 998217). Work at King's College London was supported by the Wellcome Trust (Grants 101126/Z/13/Z and 101126/B/13/Z) and in part by the National Institute for Health Research Health Protection Research Unit (NIHR HPRU) in Health Impact of Environmental Hazards at King's College London in partnership with Public Health England (PHE) and Imperial College London. The views expressed are those of the authors and not necessarily those of the National Health Service, the NIHR, the Department of Health & Social Care or PHE.

Legend to Figures

Fig. 1. Scheme of ellipticine metabolism by CYPs (in the presence [+] or absence [-] of cytochrome b_5 [b_5]) and peroxidases showing the identified metabolites and those proposed to form DNA adducts. The compounds shown in brackets were not detected under the experimental conditions and/or not structurally characterized.

Fig. 2. Scheme of preparation of ApoElli nanoparticles.

Fig. 3. (**A**) TEM micrographs of apoferritin (a), the freshly prepared ApoElli nanocarrier (b) and the ApoElli nanocarrier stored for 28 days at 4°C (c). (**B**,**C**) Size, polydispersive index and zeta potentials of Apo and ApoElli nanocarriers. Values in (**C**) are mean ± SD from six independent experiments.

Fig. 4. The ApoElli stability at +4°C (red) and –20°C (blue) in panel **A**. Values are mean ± SD from three independent experiments. $^{**}p < 0.01$ significant differences of stability of ApoElli nanoparticles without incubations (t = 0 day) (ANOVA with post-hoc Tukey HSD Test). (**B**) The kinetics of ellipticine release from ApoElli at pH 6.5 and 7.4 at 37°C. Values are mean ± SD from three independent experiments.

Fig. 5. (**A**) The effect of pH on testosterone 6-β-hydroxylation catalysed by human CYP3A4 co-expressed with cytochrome b_5 in Supersomes^{TM}. Values are mean ± SD (pmol 6-β-testosterone/CYP3A4/min) from three independent experiments. ND, not detected. (**B**) Amounts of ellipticine metabolites generated from free ellipticine (Elli) and ApoElli by human CYP3A4 co-expressed with cytochrome b_5 in Supersomes^{TM} in the presence of NADPH. Values are mean ± SD (pmol 9-hydroxy-, 12-hydroxy and/or 13-hydroxyellipticine/CYP3A4/min) from three independent *in vitro* incubations. Control – control incubation without NADPH. $^{***}p < 0.001$ significant differences between ellipticine metabolite formation at pH 7.4 and 6.5 (ANOVA with post-hoc Tukey HSD Test). (**C**) Amounts of ellipticine-derived DNA adduct 1 generated from free ellipticine (Elli) and ApoElli by human CYP3A4 co-expressed with cytochrome b_5 in Supersomes^{TM} in the presence of NADPH determined by ^{32}P-postlabeling. Values are mean ± SD from three independent *in vitro* incubations. Control – control incubation without NADPH. RAL, relative adduct labeling. $^{***}p < 0.001$ significant differences between ellipticine-DNA adduct formation at pH 7.4 and 6.5; $^{\Delta\Delta\Delta}$ $p < 0.001$ significant differences between ellipticine-DNA adduct formation by free

ellipticine and its ApoElli form (ANOVA with post-hoc Tukey HSD Test). *Insert:* Autoradiographic profiles of DNA adducts generated by free ellipticine (a) and ApoElli (b) in the CYP3A4 Supersomal system. Adduct spot 1 is formed in deoxyguanosine residues of DNA by the ellipticine metabolite 13-hydroxyellipticine.

Fig. 6. The amounts of ellipticine (nmol) determined in liposomes after its transfer from ApoElli into these liposomes and in supernatant containing residual ApoElli (full incubation). In control incubation, sediment corresponded to precipitated ApoElli. In this precipitate and the residual supernatant the amounts ellipticine was also determined. See experimental conditions for details.

Fig. 7. (**A**) Expression of SCARA5 in neuroblastoma UKF-NB-4 and non-malignant HDFn cells. (**a**) Western blot analysis of SCARA5 expression in UKF-NB-4 and HDFn cells. A representative image of the Western blotting is shown; (**b**) Western blot analysis of GAPDH protein expression in UKF-NB-4 and HDFn cells was used as a loading control; (**c**) Relative SCARA5 expression compared with GAPDH in UKF-NB-4 and HDFn cells. (**B**) Subcellular location of ellipticine (Elli) after 2 hours exposure of neuroblastoma UKF-NB-4 and non-malignant HDFn cells to 10 μM ellipticine and with the same concentration of ellipticine loaded apoferritin (ApoElli); 1 – membrane, 2 – nucleus, 3 – cytoplasm. (**C**) Fluorescence intensities (RFU, relative fluorescence units) of ellipticine in the whole cells. (**D**) Fluorescence intensities of ellipticine in cell nuclei. Values are mean ± SD from three independent experiments. ** $p < 0.01$ significant differences between fluorescence intensity in UKF-NB-4 and HDFn cells; $^{\Delta\Delta}$ $p < 0.01$ significant differences between fluorescence intensity in UKF-NB-4 and HDFn cells treated with free ellipticine (Elli) and ApoElli (ANOVA with post-hoc Tukey HSD Test).

Fig. 8. (**A**,**B**) Cytotoxicity (viable cells as percentage of control) in neuroblastoma UKF-NB-4 (**A**) and fibroblastic HDFn (**B**) cells treated with free ellipticine (Elli) and ApoElli for 48 hour determined by the AlamarBlue assay. Values are mean ± SD from three independent experiments. (**C**,**D**) Apoptosis in neuroblastoma UKF-NB-4 (**C**) and HDFn (**D**) cells induced by free ellipticine (Elli) and ApoElli. Values are mean ± SD from three independent experiments. *** $p < 0.001$, ** $p < 0.01$, significant differences between cells treated with free ellipticine and its ApoElli form and control (untreated) cells (ANOVA with post-hoc Tukey HSD Test). (**E,F**) Cell cycle distributions in UKF-NB-4 (**E**) and HDFn (**F**) cells induced by free ellipticine (Elli) and ApoElli. Values are mean ± SD from three independent experiments.

*** $p < 0.001$, ** $p < 0.01$, * $p < 0.05$, significant differences between cells treated with free ellipticine or ApoElli and control (untreated) cells (ANOVA with post-hoc Tukey HSD Test). (**G**) Haemocompatibility assay of presented nanocarriers using RBC. ApoElli at various concentrations (ellipticine concentrations of 0; 6.3; 12.5; 25; 50 and 100 μM) was mixed in 1:1 volume ratio with washed RBC diluted in PBS and incubated for 1 hour at 37°C. Lysed erythrocytes absorbance (540 nm) was measured with evaluated percentage of haemolytic RBC with ambient light visualization of the haemolytic RBC.

Fig. 9. Cell index of neuroblastoma UKF-NB-4 cells treated with free ellipticine (Elli) and ApoElli. Representative data from one of three independent experiments are shown.

Fig. 10. (**A**) Analysis of phosphorylated H2AX (γH2AX) in neuroblastoma UKF-NB-4 and fibroblastic HDFn cells induced by ellipticine (Elli) and ApoElli. Values are mean ± SD from three independent experiments. ** $p < 0.01$, significant differences between UKF-NB-4 cells treated with free ellipticine and ApoElli. $^{\Delta\Delta\Delta}$ $p < 0.001$ significant differences between UKF-NB-4 and HDFn cells (ANOVA with post-hoc Tukey HSD Test). (**B**) Ellipticine-derived DNA adduct formation in neuroblastoma UKF-NB-4 cells treated with 5 μM ellipticine (Elli) and 5 μM ApoElli determined by ^{32}P-postlabeling. Values of relative adduct labelling are expressed as adducts per 10^6 normal nucleotides. Values represent mean ± SD from three independent experiments. * $p < 0.05$, significant differences between levels of ellipticine-DNA adducts in UKF-NB-4 cells treated with free ellipticine and ApoElli (ANOVA with post-hoc Tukey HSD Test). *Insert*: Autoradiographic profiles DNA adducts formed in UKF-NB-4 cells exposed to free ellipticine (**a**) and ApoElli (**b**) determined by ^{32}P-postlabeling. Adduct spots 1 and 2 are formed in deoxyguanosine residues of DNA by the ellipticine metabolites 13-hydroxy- and 12-hydroxyellipticine, respectively.

References

Ali, I., Rahis-Uddin, Salim, K., Rather, M.A., Wani, W.A. and Haque, A. 2011 Advances in nano drugs for cancer chemotherapy. Curr. Cancer Drug Targets 11, 135-146.

Appelbe, O.K., Zhang, Q., Pelizzari, C.A., Weichselbaum, R.R. and Kron, S.J. 2016 Image-guided radiotherapy targets macromolecules through altering the tumor microenvironment. Mol. Pharm. 13, 3457-3467.

Auclair, C. 1987. Multimodal action of antitumor agents on DNA: The ellipticine series. Arch. Biochem. Biophys. 259, 1-14.

Blazkova, I., Nguyen, H.V., Dostalova, S., Kopel, P., Stanisavljevic, M., Vaculovicova, M., Stiborova, M., Eckschlager, T., Kizek, R. and Adam, V. 2013 Apoferritin modified magnetic particles as doxorubicin carriers for anticancer drug delivery. Int. J. Mol. Sci.14, 13391-13402.

Bořek-Dohalská, L., Hodek, P., Sulc, M. and Stiborová, M. 2001 Alpha-Naphthoflavone acts as activator and reversible or irreversible inhibitor of rabbit microsomal CYP3A6. Chem. Biol. Interact. 138, 85-106.

Bořek-Dohalská, L. and Stiborová, M. 2010 Cytochrome P450 3A activities and their modulation by alpha-naphthoflavone *in vitro* are dictated by the efficiences of model experimental systems. Coll. Czech. Chem. Commun. 75, 201-220.

Chomoucka, J., Drbohlavova, J., Huska, D., Adam, V., Kizek, R. and Hubalek, J. 2010 Magnetic nanoparticles and targeted drug delivering. Pharmacol. Res. 62, 144-149.

Clogston, J.D. and Patri, A.K. 2011 Zeta potential measurement. Methods. Mol. Biol. 697, 63-70.

Corbet, C. and Feron, O. 2017 Tumour acidosis: from the passenger to the driver's seat. Nat. Rev. Cancer 17, 577-593.

Dostalova, S., Cerna, T., Hynek, D., Koudelkova, Z., Vaculovic, T., Kopel, P., Hrabeta, J., Heger, Z., Vaculovicova, M., Eckschlager, T., Stiborova, M. and Adam, V 2016 Site-directed conjugation of antibodies to apoferritin nanocarrier for targeted drug delivery to prostate cancer cells. ACS Appl. Mater. Interfaces 8, 14430-14441.

Dostalova, S., Vasickova, K., Hynek, D., Krizkova, S., Richtera, L., Vaculovicova, M., Eckschlager, T., Stiborova, M., Heger, Z. and Adam, V. 2017 Apoferritin as an ubiquitous nanocarrier with excellent shelf life. Int. J. Nanomed. 12, 2265-2278.

Frei, E., Bieler, C.A., Arlt, V.M., Wiessler, M. and Stiborová, M. 2002. Covalent binding of the anticancer drug ellipticine to DNA in V79 cells transfected with human cytochrome P450 enzymes. Biochem. Pharmacol. 64, 289-295.

Gallois, B., dEstaintot, B.L., Michaux, M.A., Dautant, A., Granier, T., Precigoux, G., Soruco, J.A., Roland, F., Chavas-Alba, O., Herbas, A. and Crichton, R.R. 1997 X-Ray structure of recombinant horse L-chain apoferritin at 2.0 angstrom resolution: implications for stability and function. J. Biol. Inorg. Chem. 2, 360-367.

Garbett, N.C. and Graves, D.E. 2004 Extending nature's leads: the anticancer agent ellipticine. Curr. Med. Chem. Anti-Cancer Agents 4, 149-172.

Gaumet, M., Vargas, A., Gurny, R. and Delie, F. 2008 Nanoparticles for drug delivery: the need for precision in particle size parameters. Eur. J. Pharm. Biopharm. 69, 1-9.

Gavvala, K., Koninci, R.K., Sengupta, A. and Hazra, P. 2014 Excited state proton transfer dynamics of an eminent anticancer drug, ellipticine, in octyl glucoside micelle. Phys. Chem. Chem. Phys. 16, 14953-14960.

Goswami, S.R., Sahareen, T., Singh, M. and Kumar, S. 2015 Role of biogenic silver nanoparticles in disruption of cell-cell adhesion in *Staphylococcus aureus* and *Escherichia coli* biofilm. J. Ind. Eng. Chem. 26, 73-80.

Heger, Z., Skalickova, S., Zitka, O., Adam, V. and Kizek, R. 2014 Apoferritin applications in nanomedicine. Nanomedicine 9, 2233-2245.

Hrabeta, J., Groh, T., Khalil, M.A., Poljakova, J., Adam, V., Kizek, R., Uhlik, J., Doktorova, H., Cerna, T., Frei, E., Stiborova, M. and Eckschlager, T. 2015 Vacuolar-ATPase-mediated intracellular sequestration of ellipticine contributes to drug resistance in neuroblastoma cells. Int. J. Oncol. 47, 971-980.

Kamath, S.A., Kummerow, F.A. and Narayan, K.A. 1971 A simple procedure for the isolation of rat liver microsomes. FEBS Lett. 17, 90-92.

Ke, N., Wang, X., Xu, X. and Abassi, Y.A. 2011 The xCELLigence system for real-time and label-free monitoring of cell viability. Methods Mol. Biol. 740, 33-43.

Kilic, M.A., Ozlu, E. and Calis, S. 2012 A novel protein-based anticancer drug encapsulating nanosphere: apoferritin-doxorubicin complex. J. Biomed. Nanotechnol. 8, 508-514.

Kim, M.S., Blake, M., Baek, J.H., Kohlhagen, G., Pommier, Y. and Carrier, F. 2003 Inhibition of histone deacetylase increases cytotoxicity to anticancer drugs targeting DNA. Cancer Res. 63, 7291-7300.

Kim, M., Rho, Y., Jin, K.S., Ahn, B., Jung, S., Kim, H. and Ree, M. 2011 pH-dependent structures of ferritin and apoferritin in solution: disassembly and reassembly. Biomacromolecules 12, 1629-1640.

Kizek, R., Adam, V., Hrabeta, J., Eckschlager, T., Smutny, S., Burda, J.V., Frei, E. and Stiborova, M. 2012 Anthracyclines and ellipticines as DNA-damaging anticancer drugs: recent advances. Pharmacol. Ther. 133, 26-39.

Kotrbová, V., Mrázová, B., Moserová, M., Martínek, V., Hodek, P., Hudeček, J., Frei, E. and Stiborová, M. 2011 Cytochrome b_5 shifts oxidation of the anticancer drug ellipticine by cytochromes P450 1A1 and 1A2 from its detoxication to activation, thereby modulating its pharmacological efficacy. Biochem. Pharmacol. 82, 669-680.

Krausova, K. 2017 Study of expression of transferrin receptors (TfR1) and their utilization in nanomedicine (in Czech), Bachelor Thesis, Brno University of Technology, Brno, Czech Republic.

Kulkarni, P.R., Yadav, J.D. and Vaidya, K.A. 2011 Liposomes: a novel drug delivery system. Int. J. Curr. Pharm. Res. 3, 10-18.

Liang, M., Fan, K., Zhou, M., Duan, D., Zheng, J., Yang, D., Feng, J. and Yan, X. 2014 H-ferritin-nanocaged doxorubicin nanoparticles specifically target and kill tumors with a single-dose injection. Proc. Natl. Acad. Sci. U. S. A. 111, 14900-14905.

Liu, K., Dai, L., Li, C., Liu, J., Wang, L. and Lei, J. 2016 Self-assembled targeted nanoparticles based on transferrin-modified eight-arm-polyethylene glycol-dihydroartemisinin conjugate. Sci. Rep. 6, 29461.

Martínek, V., Sklenár, J., Dracínsky, M., Sulc, M., Hofbauerová, K., Bezouska, K., Frei, E. and Stiborová, M. 2010 Glycosylation protects proteins against free radicals generated from toxic xenobiotics. Toxicol. Sci. 117, 59-74.

Mendes-Jorge, L., Ramos, D., Valença, A., López-Luppo, M., Pires, V.M., Catita, J., Nacher, V., Navarro, M., Carretero, A,, Rodriguez-Baeza, A. and Ruberte, J. 2014 L-ferritin binding to SCARA5: a new iron traffic pathway potentially implicated in retinopathy. PLoS One 9, e106974.

Moore, T.L., Rodriguez-Lorenzo, L., Hirsch, V., Balog, S., Urban, D., Jud, C., Rothen-Rutishauser, B., Lattuada, M. and Petri-Fink, A. 2015 Nanoparticle colloidal stability in cell culture media and impact on cellular interactions. Chem. Soc. Rev. 44, 6287-305.

Nakamura, A.J., Rao, V.A., Pommier, Y. and Bonner, W.M. 2010 The complexity of phosphorylated H2AX foci formation and DNA repair assembly at DNA double-strand breaks. Cell Cycle 9, 389-397.

Nakamura, Y., Nakamichi, N., Takarada, T., Ogita, K and, Yoneda, Y. 2012 Transferrin receptor-1 suppresses neurite outgrowth in euroblastoma Neuro2A Cells. Neurochem. Int. 60,448-457.

Petros, R.A. and DeSimone, J.M. 2010 Strategies in the design of nanoparticles for therapeutic applications. Nat. Rev. Drug Discovery 9, 615-627.

Plch, J., Venclikova, K., Janouskova, O., Hrabeta, J., Eckschlager, T., Kopeckova, K., Hampejsova, Z., Bosakova, Z., Sirc, J. and Hobzova, R. 2018 Paclitaxel-loaded polylactide/polyethylene glycol fibers with long-term antitumor activity as a potential drug carrier for local chemotherapy. Macromol. Biosci. 18, e1800011.

Poljaková, J., Frei, E., Gomez, J.E., Aimová, D., Eckschlager, T., Hraběta, J. and Stiborová, M. 2007. DNA adduct formation by the anticancer drug ellipticine in human leukemia HL-60 and CCRF-CEM cells. Cancer Lett. 252, 270-279.

Poljaková, J., Eckschlager, T., Hraběta, J., Hrebacková, J., Smutný, S., Frei, E., Martínek, V., Kizek, R. and Stiborová, M. 2009 The mechanism of cytotoxicity and DNA adduct formation by the anticancer drug ellipticine in human neuroblastoma cells. Biochem. Pharmacol. 77, 1466-1479.

Poljakova, J., Hrebackova, J., Dvorakova, M., Moserova, M., Eckschlager, T., Hrabeta, J., Göttlicherova, M., Kopejtkova, B., Frei, E., Kizek. R. and Stiborova, M. 2011 Anticancer agent ellipticine combined with histone deacetylase inhibitors, valproic acid and trichostatin A, is an effective DNA damage strategy in human neuroblastoma. Neuro Endocrinol. Lett. 32, 101-116.

Procházka, P., Libra, A., Zemanová, Z., Hřebačková, J., Poljaková, J., Hraběta, J., Bunček, M., Stiborová, M. and Eckschlager, T. 2012 Mechanisms of ellipticine-mediated resistance in UKF-NB-4 neuroblastoma cells. Cancer Sci. 103, 334-341.

Ryvolova, M., Chomoucka, J., Drbohlavova, J., Kopel, P., Babula, P., Hynek, D., Adam, V., Eckschlager, T., Hubalek, J., Stiborova, M., Kaiser, J. and Kizek, R. 2012 Modern micro and nanoparticle-based imaging techniques. Sensors 12, 14792-14820.

Schmeiser, H.H., Stiborova, M. and Arlt, V.M. 2013 ^{32}P-Postlabeling analysis of DNA adducts. Methods Mol Biol 1044, 389-401.

Sedlacek, O., Studenovsky, M., Vetvicka, D., Ulbrich, K. and Hruby, M. 2013 Fine tuning of the pH-dependent drug release rate from polyHPMA-ellipticinium conjugates. Bioorg. Med. Chem. 21, 5669-5672.

Sharma, A., Singh, K. and Almasan, A. 2012 Histone H2AX phosphorylation: a marker for DNA damage. Methods Mol. Biol. 920, 613-626.

Stiborová, M., Bieler, C.A., Wiessler, M. and Frei, E. 2001. The anticancer agent ellipticine on activation by cytochrome P450 forms covalent DNA adducts. Biochem. Pharmacol. 62,675-684.

Stiborová, M., Breuer, A., Aimová, D., Stiborová-Rupertová, M., Wiessler, M. and Frei, E. 2003a. DNA adduct formation by the anticancer drug ellipticine in rats determined by ^{32}P-postlabeling. Int. J. Cancer 107, 885-890.

Stiborová, M., Stiborová-Rupertová, M., Bořek-Dohalská, L., Wiessler, M. and Frei, E. 2003b. Rat microsomes activating the anticancer drug ellipticine to species covalently binding to deoxyguanosine in DNA are a suitable model mimicking ellipticine bioactivation in humans. Chem. Res. Toxicol. 16, 38-47.

Stiborová, M., Sejbal, J., Bořek-Dohalská, L., Aimová, D., Poljaková, J., Forsterová, K., Rupertová, M., Wiesner, J., Hudeček, J., Wiessler, M. and Frei, E. 2004. The anticancer drug ellipticine forms covalent DNA adducts, mediated by human cytochromes P450, through metabolism to 13-hydroxyellipticine and ellipticine N^2-oxide. Cancer Res. 64, 8374-8380.

Stiborová, M., Rupertová, M., Schmeiser, H.H. and Frei, E. 2006 Molecular mechanism of antineoplastic action of an anticancer drug ellipticine. Biomed. Pap. Med. Fac. Univ. Palacky Olomouc Czech Repub. 150, 13-23.

Stiborová, M., Poljaková, J., Ryšlavá, H., Dračínský, M., Eckschlager, T. and Frei, E., 2007a. Mammalian peroxidases activate anticancer drug ellipticine to intermediates forming

deoxyguanosine adducts in DNA identical to those found *in vivo* and generated from 12-hydroxyellipticine and 13-hydroxyellipticine. Int. J. Cancer 120, 243-251.

Stiborová, M., Rupertová, M., Aimová, D., Ryšlavá, H. and Frei, E. 2007b. Formation and persistence of DNA adducts of anticancer drug ellipticine in rats. Toxicology 236, 50-60.

Stiborová, M., Arlt, V.M., Henderson, C.J., Wolf, C.R., Kotrbová, V., Moserová, M., Hudeček, J., Phillips, D.H. and Frei, E. 2008 Role of hepatic cytochromes P450 in bioactivation of the anticancer drug ellipticine: studies with the hepatic NADPH:cytochrome P450 reductase null mouse. Toxicol. Appl. Pharmacol. 226, 318-327.

Stiborová, M., Rupertová, M. and Frei, E. 2011 Cytochrome P450- and peroxidase-mediated oxidation of anticancer alkaloid ellipticine dictates its anti-tumor efficiency. Biochim. Biophys. Acta - Proteins and Proteomics 1814, 175-185.

Stiborová, M., Indra, R., Moserová, M., Cerná, V., Rupertová, M., Martínek, V., Eckschlager, T., Kizek, R. and Frei, E. 2012a Cytochrome b_5 increases cytochrome P450 3A4-mediated activation of anticancer drug ellipticine to 13-hydroxyellipticine whose covalent binding to DNA is elevated by sulfotransferases and N,O-acetyltransferases. Chem. Res. Toxicol. 25, 1075-1085.

Stiborová, M., Poljaková, J., Martínková, E., Ulrichová, J., Simánek, V., Dvořák, Z. and Frei, E. 2012b Ellipticine oxidation and DNA adduct formation in human hepatocytes is catalyzed by human cytochromes P450 and enhanced by cytochrome b_5. Toxicology 302, 233-241.

Stiborova, M. and Frei, E. 2014 Ellipticines as DNA-targeted chemotherapeutics. Current Med. Chem. 21, 575-591.

Stiborova, M., Manhartova, Z., Hodek, P., Adam, V., Kizek, R. and Frei, E. 2014a Formation of DNA adducts by ellipticine and its micellar form in rats - a comparative study. Sensors 14, 22982-22997.

Stiborová, M., Poljaková, J., Mrizova, I., Borek-Dohalska, L., Eckschlager, T., Adam, V., Kizek, R. and Frei, E. 2014b Expression levels of enzymes metabolizing an anticancer drug ellipticine determined by electromigration assays influence its cytotoxicity to cancer cells - a comparative study. Int. J. Electrochem. Sci. 9, 5675-5689.

Stiborová, M., Černá, V., Moserová, M., Mrízová, I., Arlt, V.M. and Frei, E. 2015a The anticancer drug ellipticine activated with cytochrome P450 mediates DNA damage determining its pharmacological efficiencies: studies with rats, hepatic cytochrome P450 reductase null (HRN™) mice and pure enzymes. Int. J. Mol. Sci. 16, 284-306.

Stiborova, M., Manhartova, Z., Hodek, P., Adam, V., Kizek, R., Eckschlager, T. and Frei, E. 2015b Cytotoxicity of and DNA adduct formation by ellipticine and its micellar form in human leukemia cells *in vitro*. Neuro Endocrinol. Lett. 36 (Suppl. 1), 22-28.

Stiborová, M., Indra, R., Frei, E., Kopečková, K., Schmeiser, H.H., Eckschlager, T., Adam, V., Heger, Z., Arlt, V.M. and Martínek,V. 2017 Cytochrome b_5 plays a dual role in the reaction cycle of cytochrome P450 3A4 during oxidation of the anticancer drug ellipticine. Monatsh. Chem. 148, 1983-1991.

Studenovský, M., Sedláček, O., Hrubý, M., Pánek, J. and Ulbrich, K. 2015 Multi responsive polymer micelles as ellipticine delivery carriers for cancer therapy. Anticancer Res. 35, 753-757.

Stylianopoulos, T. and Jain, R.K. 2015 Design considerations for nanotherapeutics in oncology. Nanomed. Nanotechnol. Biol. Med. 11, 1893-1907.

Svenson, S. 2012 Clinical translation of nanomedicines. Curr. Opin. Solid State Mat. Sci. 16, 287-294.

Svenson, S. 2013 Theranostics: are we there yet? Mol. Pharmaceutics 10, 848-856.

Tmejova, K., Hynek, D., Kopel, P., Dostalova, S., Smerkova, K., Stanisavljevic, M., Nguyen, H.V., Nejdl, L., Vaculovicova, M., Krizkova, S., Kizek, R. and Adam, V. 2013

Electrochemical behaviour of doxorubicin encapsulated in apoferritin. Int. J. Electrochem. Sci. 8, 12658-12671.

Tmejova, K., Krejcova, L., Hynek, D., Adam, V., Babula, P., Trnková, L., Stiborova, M., Eckschlager, T. and Kizek, R. 2014 Electrochemical study of ellipticine interaction with single and double stranded oligonucleotides. Anti-Cancer Age Med. 14, 331-340.

Uchida, M., Klem, M.T., Allen, M., Suci, P., Flenniken, M., Gillitzer, E., Varpness, Z., Liepold, L.O., Young, M. and Douglas, T. 2007 Biological containers: protein cages as multifunctional nanoplatforms. Adv. Mater. 19, 1025-1042.

Yang, H., Fung, S.Y., Pritzker, M. and Chen, P. 2007 Modification of hydrophilic and hydrophobic surfaces using an ionic-complementary peptide. PLoS One 19, e1325.

Wan, Z., Lu, S., Zhao, D., Ding, Y. and Chen, P. 2016 Arginine-rich ionic complementary peptides as potential drug carriers: impact of peptide sequence on size, shape and cell specificity. Nanomedicine 12, 1479-1488.

Wu, Y., Sadatmousavi, P., Wang, R., Lu, S., Yuan, Y.F. and Chen, P. 2012 Self-assembling peptide-based nanoparticles enhance anticancer effect of ellipticine *in vitro* and *in vivo*. Int. J. Nanomed. 7, 3221-3233.

Zhang, L., Bennett, W.F., Zheng, T., Ouyang, P.K., Ouyang, X., Qiu, X., Luo, A,, Karttunen, M, and Chen, P. 2016. Effect of cholesterol on cellular uptake of cancer drugs pirarubicin and ellipticine. J. Phys. Chem. B, 120, 148-156.

Zhang, L., Xu, J., Wang, F., Ding, Y,, Wang, T., Jin, G., Martz, M., Gui, Z., Ouyang, P. and Chen, P. 2019. Histidine-rich cell-penetrating peptide for cancer drug delivery and its uptake mechanism. Langmuir. 35, 3513-3523.

Zwelling, L.A., Michaels, S., Kerrigan, D., Pommier, Y. and Kohn, K.W. 1982 Protein-associated deoxyribonucleic acid strand breaks produced in mouse leukemia L1210 cells by ellipticine and 2-methyl-9-hydroxyellipticinium. Biochem. Pharm. 31, 3261-3267.

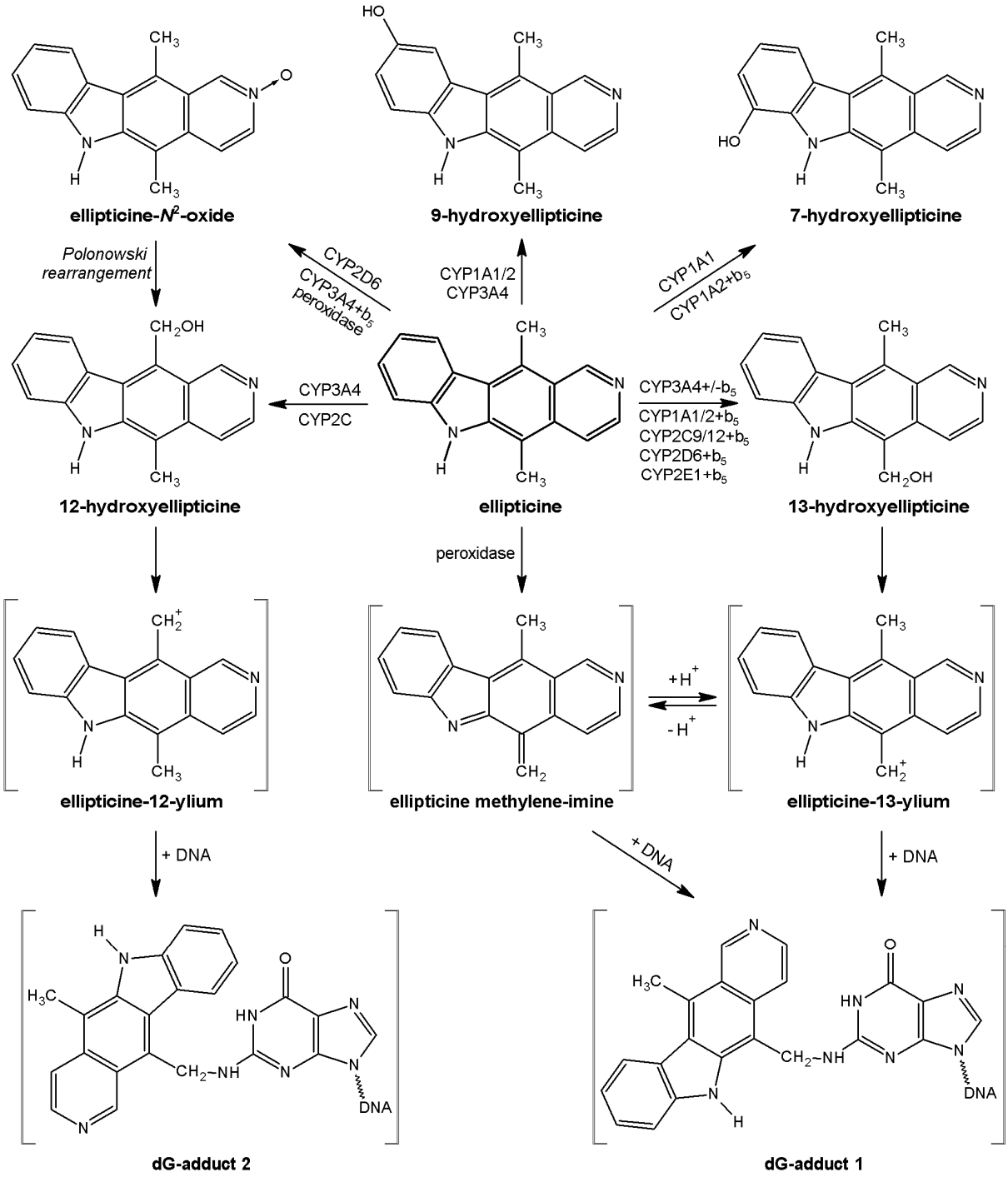
ellipticine-N2-oxide
9-hydroxyellipticine
7-hydroxyellipticine
Polonowski rearrangement
CYP2D6
CYP3A4+b5
peroxidase
CYP1A1/2
CYP3A4
CYP1A1
CYP1A2+b5
12-hydroxyellipticine
CYP3A4
CYP2C
ellipticine
CYP3A4+/-b5
CYP1A1/2+b5
CYP2C9/12+b5
CYP2D6+b5
CYP2E1+b5
13-hydroxyellipticine
peroxidase
ellipticine-12-ylium
ellipticine methylene-imine
+H+
-H+
ellipticine-13-ylium
+ DNA
+ DNA
+ DNA
dG-adduct 2
dG-adduct 1

Fig. 1.

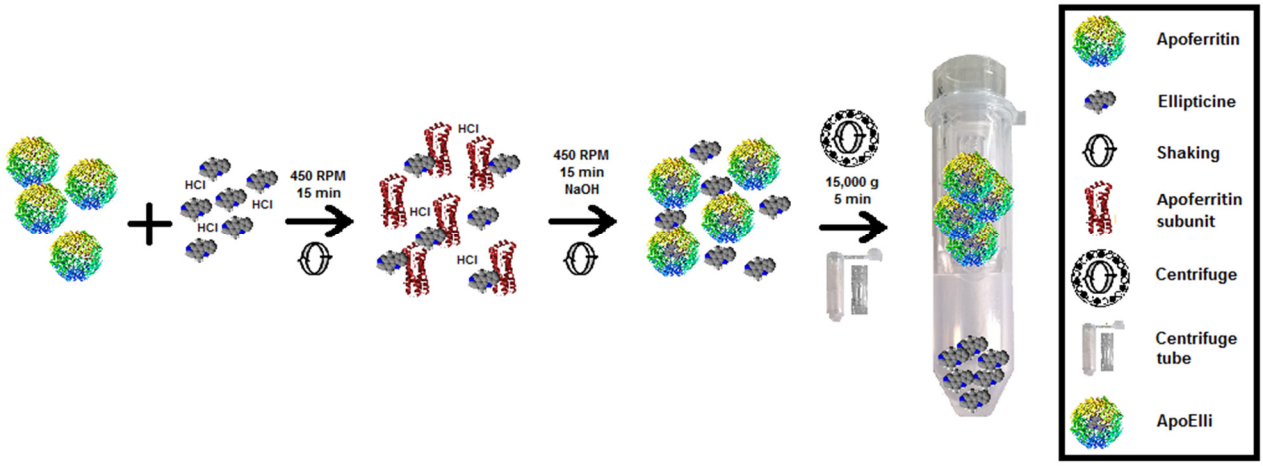
HCl
HCl
HCl
450 RPM
15 min
HCl
HCl
HCl
450 RPM
15 min
NaOH
15,000 g
5 min
Apoferritin
Ellipticine
Shaking
Apoferritin subunit
Centrifuge
Centrifuge tube
ApoElli

Fig. 2.

A

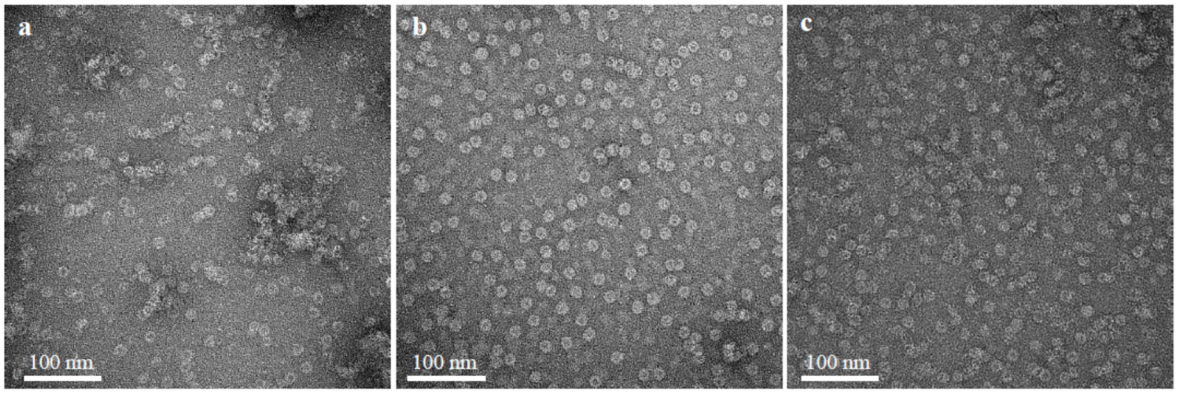

B

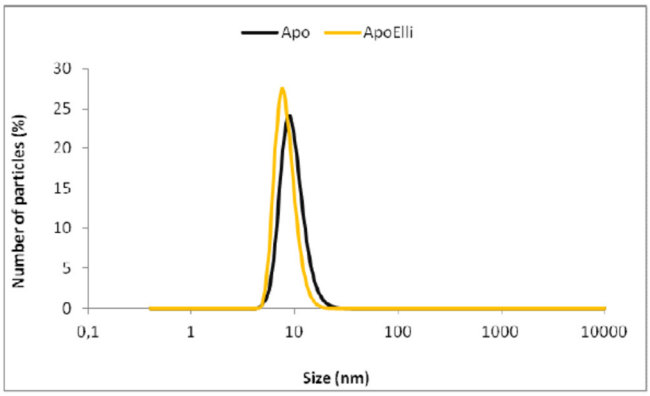

C

Nanocarrier	Apo	ApoElli
Size (nm)	11.7 ± 0.31	10.1 ± 0.57
Polydispersive index	0.350 ± 0.09	0.419 ± 0.24
Zeta potential (mV)	-32.0 ± 2.02	-36.2 ± 2.65

Fig. 3.

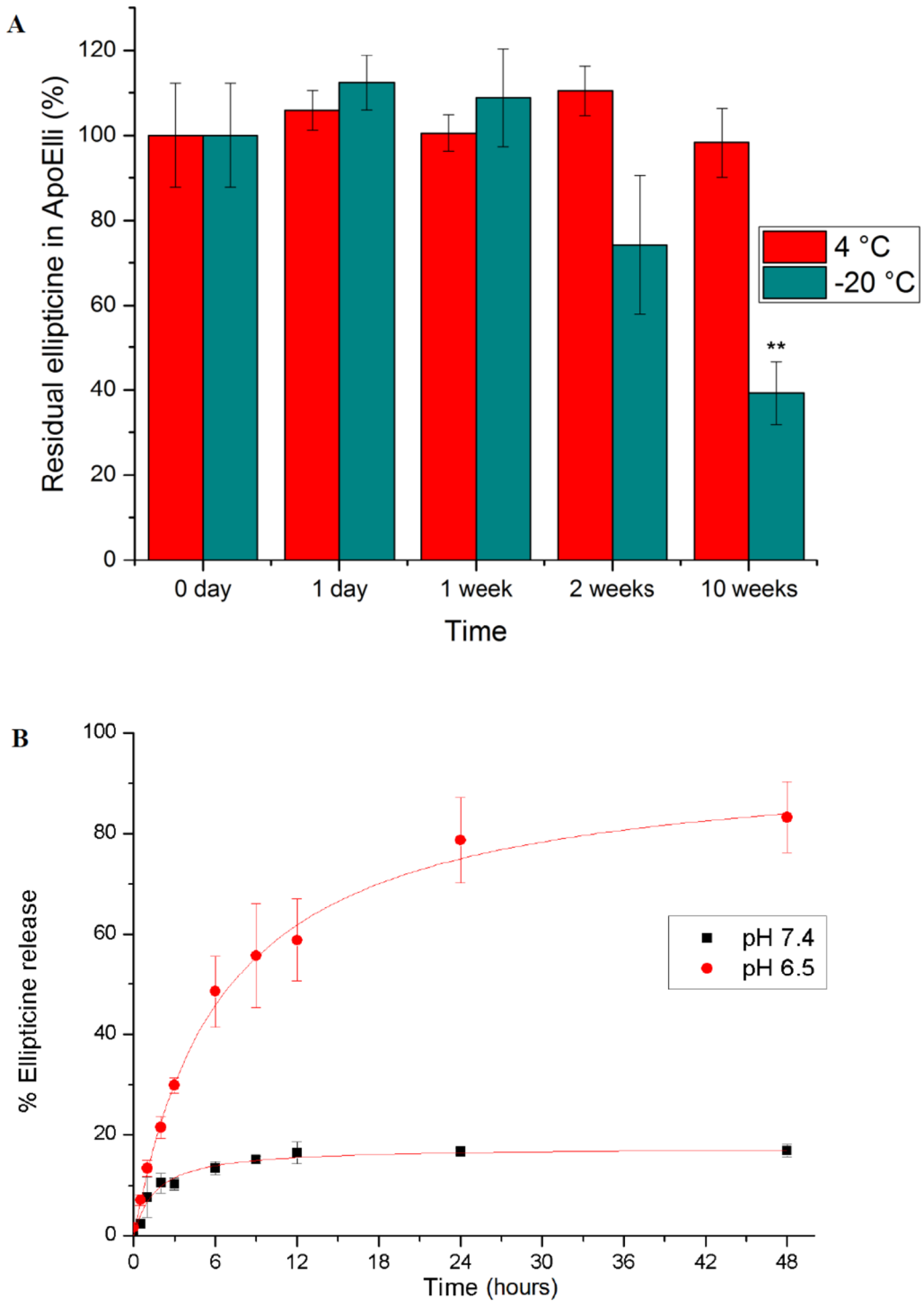
A
Residual ellipticine in ApoElli (%)
120
100
80
60
40
20
0
0 day
1 day
1 week
2 weeks
10 weeks
Time
4 °C
-20 °C
**
B
% Ellipticine release
100
80
60
40
20
0
0
6
12
18
24
30
36
42
48
Time (hours)
pH 7.4
pH 6.5

Fig. 4.

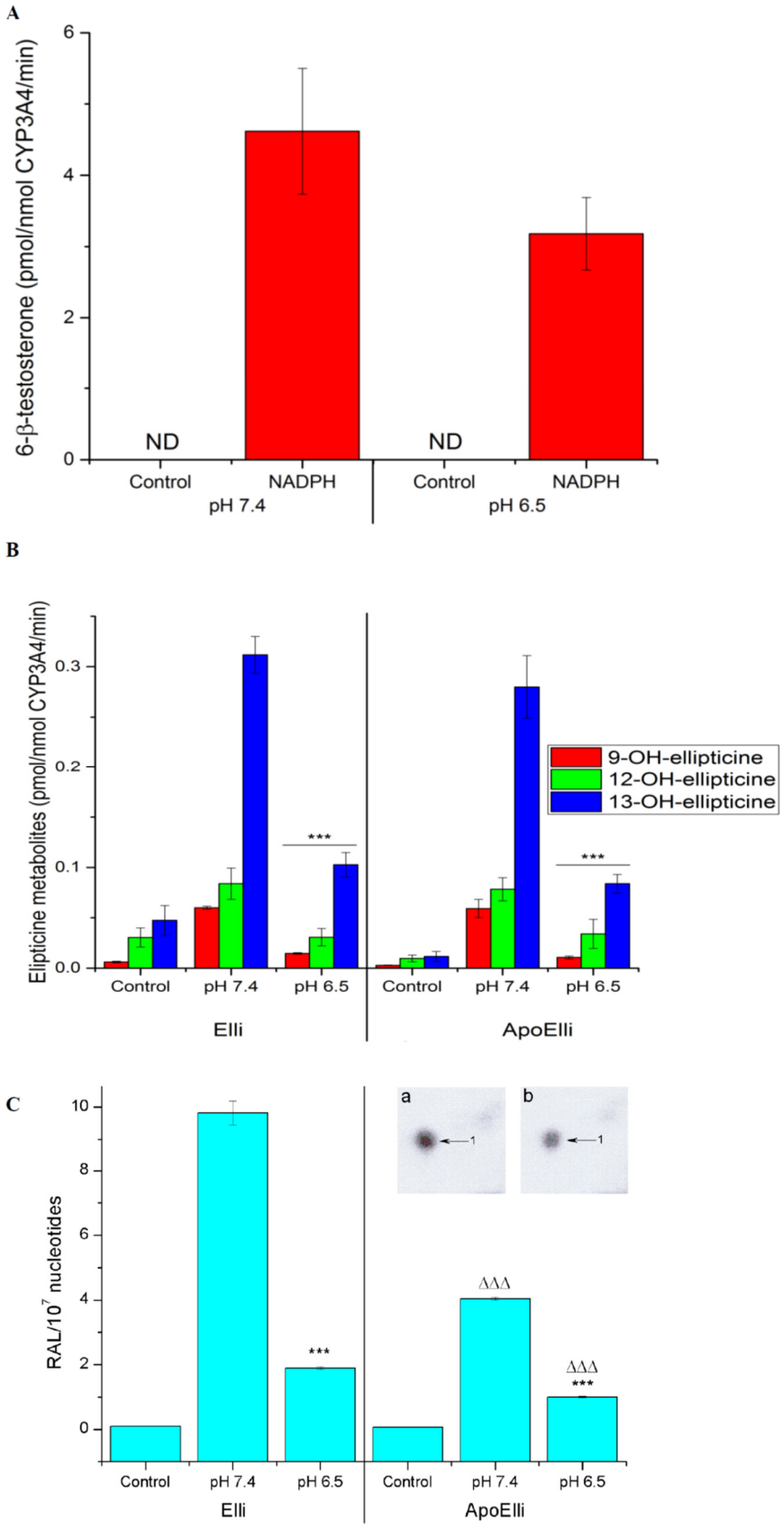
A
6-β-testosterone (pmol/nmol CYP3A4/min)
ND
ND
Control
NADPH
Control
NADPH
pH 7.4
pH 6.5
B
Elipticine metabolites (pmol/nmol CYP3A4/min)
9-OH-ellipticine
12-OH-ellipticine
13-OH-ellipticine
***
***
Control
pH 7.4
pH 6.5
Control
pH 7.4
pH 6.5
Elli
ApoElli
C
RAL/10^7 nucleotides
a
b
ΔΔΔ
***
ΔΔΔ
***
Control
pH 7.4
pH 6.5
Control
pH 7.4
pH 6.5
Elli
ApoElli

Fig. 5.

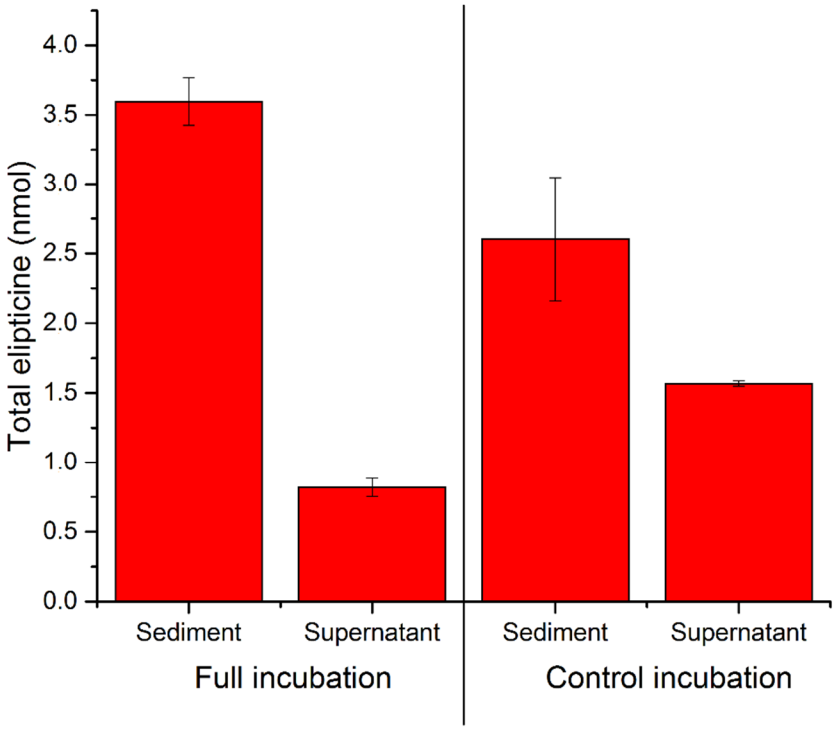
Total elipticine (nmol)
4.0
3.5
3.0
2.5
2.0
1.5
1.0
0.5
0.0
Sediment
Supernatant
Sediment
Supernatant
Full incubation
Control incubation

Fig. 6.

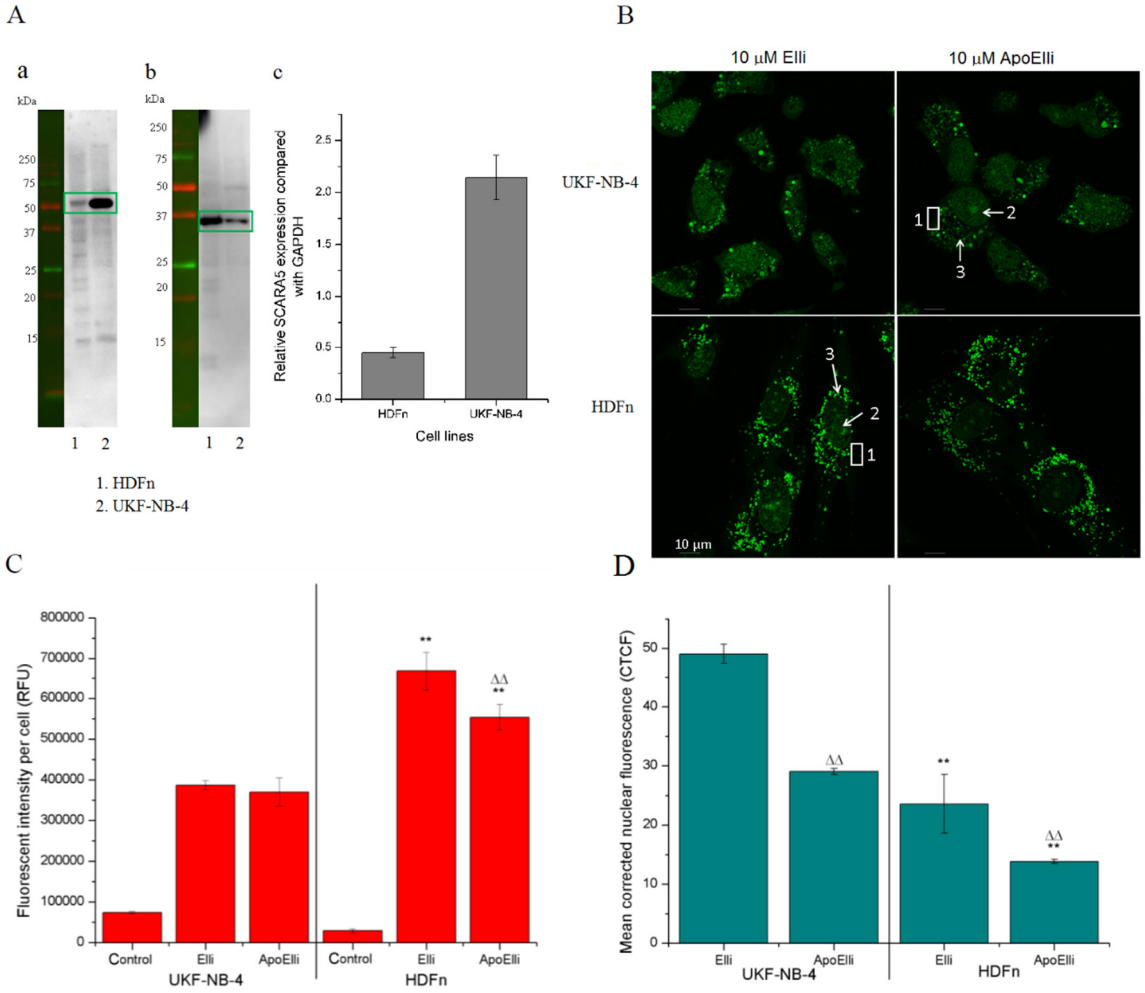
A
a
b
c
kDa
250
75
50
37
25
20
15
1 2
1. HDFn
2. UKF-NB-4
Relative SCARA5 expression compared with GAPDH
HDFn
UKF-NB-4
Cell lines
B
10 μM Elli
10 μM ApoElli
UKF-NB-4
HDFn
10 μm
C
Fluorescent intensity per cell (RFU)
Control
Elli
ApoElli
UKF-NB-4
HDFn
D
Mean corrected nuclear fluorescence (CTCF)
Elli
ApoElli
UKF-NB-4
HDFn

Fig. 7.

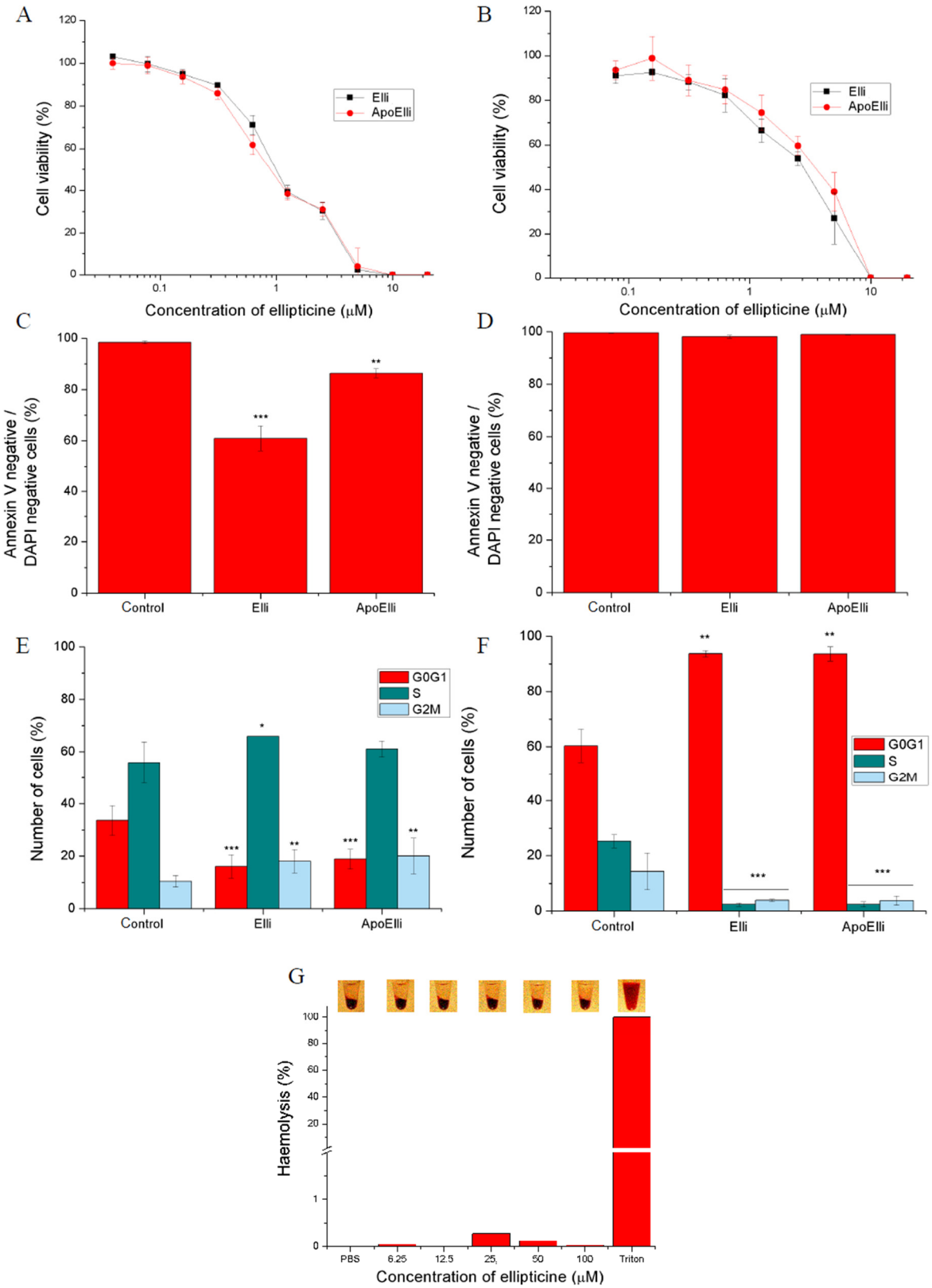
A
Cell viability (%)
Concentration of ellipticine (μM)
Elli
ApoElli
B
Cell viability (%)
Concentration of ellipticine (μM)
Elli
ApoElli
C
Annexin V negative / DAPI negative cells (%)
Control
Elli
ApoElli
D
Annexin V negative / DAPI negative cells (%)
Control
Elli
ApoElli
E
Number of cells (%)
G0G1
S
G2M
Control
Elli
ApoElli
F
Number of cells (%)
G0G1
S
G2M
Control
Elli
ApoElli
G
Haemolysis (%)
PBS
6.25
12.5
25
50
100
Triton
Concentration of ellipticine (μM)

Fig. 8.

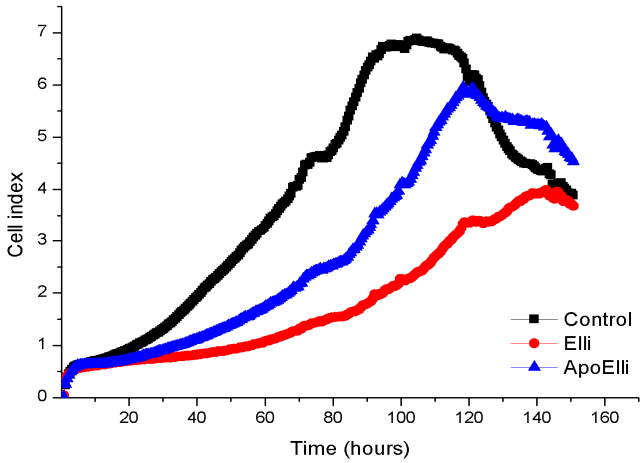
Cell index
Time (hours)
Control
Elli
ApoElli
0
1
2
3
4
5
6
7
20
40
60
80
100
120
140
160

Fig. 9.

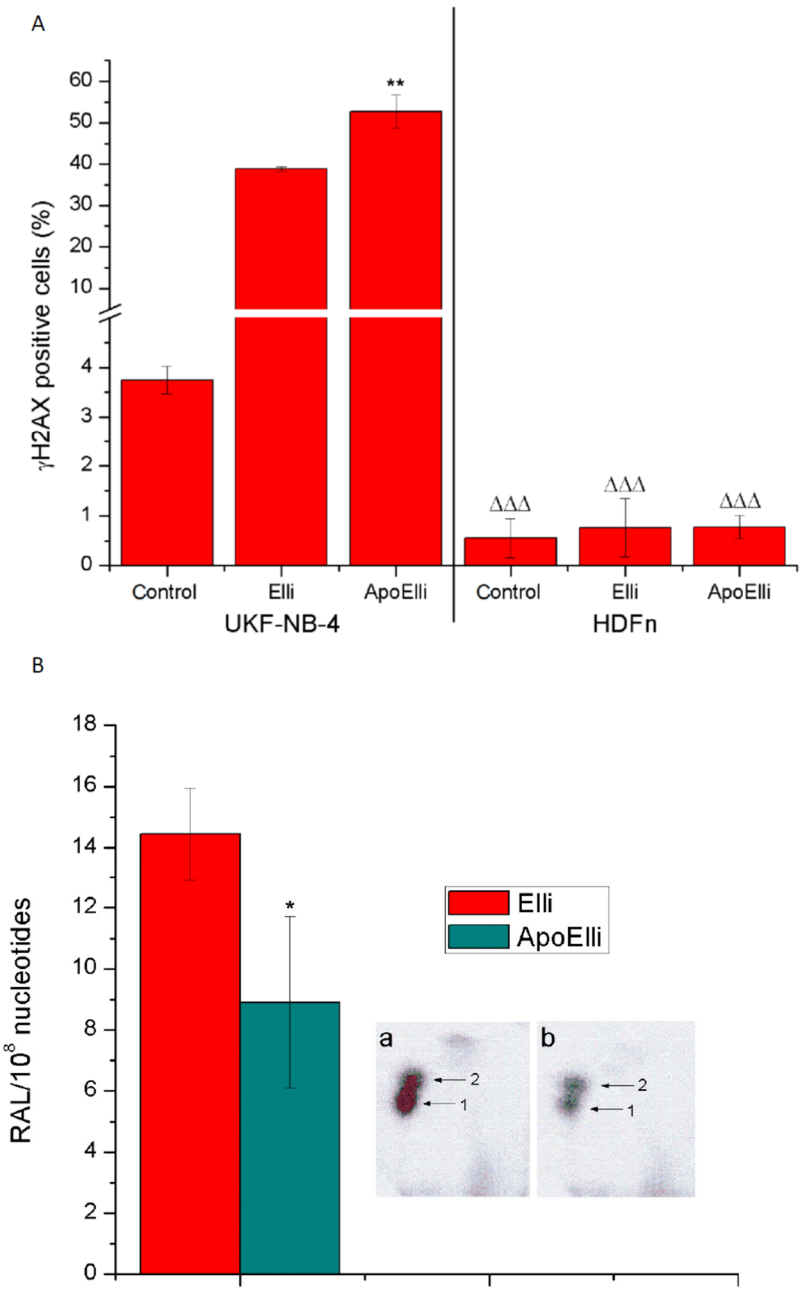
A
γH2AX positive cells (%)
60
50
40
30
20
10
4
3
2
1
0
**
ΔΔΔ
ΔΔΔ
ΔΔΔ
Control
Elli
ApoElli
Control
Elli
ApoElli
UKF-NB-4
HDFn
B
RAL/10^8 nucleotides
18
16
14
12
10
8
6
4
2
0
*
Elli
ApoElli
a
b
2
1
2
1

Fig. 10.